

## Colloidal nanocrystal quantum dot assemblies as artificial solids

Tobias Hanrath

Citation: *J. Vac. Sci. Technol. A* **30**, 030802 (2012); doi: 10.1116/1.4705402

View online: <http://dx.doi.org/10.1116/1.4705402>

View Table of Contents: <http://avspublications.org/resource/1/JVTAD6/v30/i3>

Published by the AVS: Science & Technology of Materials, Interfaces, and Processing

---

### Additional information on J. Vac. Sci. Technol. A

Journal Homepage: <http://avspublications.org/jvsta>

Journal Information: [http://avspublications.org/jvsta/about/about\\_the\\_journal](http://avspublications.org/jvsta/about/about_the_journal)

Top downloads: [http://avspublications.org/jvsta/top\\_20\\_most\\_downloaded](http://avspublications.org/jvsta/top_20_most_downloaded)

Information for Authors: [http://avspublications.org/jvsta/authors/information\\_for\\_contributors](http://avspublications.org/jvsta/authors/information_for_contributors)

### ADVERTISEMENT



AMERICAN  
ELEMENTS

**Now Invent.<sup>TM</sup>**

The World's Manufacturer  
of Engineered &  
Advanced Materials

[www.americanelements.com](http://www.americanelements.com)

## Colloidal nanocrystal quantum dot assemblies as artificial solids

Tobias Hanrath<sup>a)</sup>

School of Chemical and Biomolecular Engineering, Cornell University, Ithaca, New York 14853

(Received 9 April 2012; accepted 9 April 2012; published 3 May 2012)

The prospect of designing novel materials with electrical, optical, and magnetic properties by design has intrigued scientists and engineers for years. Building blocks for such “artificial solids” have emerged from recent advances in nanomaterial synthesis, characterization, and emerging understanding of their size-dependent properties. Colloidal semiconductor nanocrystal quantum dots (NQDs) stand out as an intellectually intriguing and experimentally advantageous system for the fundamental study of artificial solids and their technological development. The authors review the rapid evolution of artificial solids from an early theoretical concept towards the refined control of metamaterials with programmable electronic structure and their potential commercial applications, in particular, in next-generation energy technologies. The review is organized around the three independently adjustable parameters of artificial solids: (i) the electronic structure of NQD as artificial atom by tailoring the quantum confinement of the wave function, (ii) the interdot coupling as an artificial bond, and (iii) the self-assembly of NQDs into ordered superstructures as artificial crystals. The authors review elementary aspects of colloidal NQD synthesis as well as pertinent advances which have led to refined control over the NQD size, shape, and composition. Coupling between NQDs is reviewed in the context of an artificial bond; we summarize chemical and physical approaches to address the seemingly contradictory requirements of coupling nanostructures while preserving the effects of quantum-confinement. The authors review the self-assembly of NQDs into ordered superstructures in analogy to atomic crystal growth and discuss fundamental interactions between NQD and how they can be modulated to direct the growth of superlattices with predefined structures. Collectively, the experimental control over the properties of the artificial atom, bond, and crystal enable the systematic exploration of the electronic phase diagram of NQD solids. From an applied perspective, these advances have created an immensely fertile opportunity space technological applications of artificial solids in optoelectronic devices. The authors conclude with a perspective on three specific unresolved challenges ahead: (i) knowledge gaps concerning the detailed physiochemical nature of the NQD surface, (ii) limitations posed by the inherent inhomogeneity within the ensemble of NQDs, (iii) the *true* electronic structure of NQD solids, and (iv) the connection between NQD model systems in the laboratory and commercially deployable NQD technologies. © 2012 American Vacuum Society. [http://dx.doi.org/10.1116/1.4705402]

### I. INTRODUCTION

Recent advances in the synthesis and characterization of nanomaterials have created a fertile opportunity space both as an experimental platform for fundamental studies of quantum-confined properties as well as a material platform enabling potentially transformative advances in nanotechnologies. The properties of quantum-confined semiconductors have been investigated since the 1970s and theoretical and experimental studies of structures grown by high vacuum techniques, such as molecular beam epitaxy (MBE) or metal-organic vapor phase epitaxy (MOVPE), have provided valuable insight into structural and electronic properties of quantum-confined systems.<sup>1–3</sup> More recently, the discovery of wet synthesis routes of colloidal nanostructures facilitated access to a broad range of nanomaterials with controlled size, shape, and com-

position. Semiconductor nanocrystal quantum dots (NQDs), in particular, have captivated the field with potentially transformative impact on a broad range of technologies by virtue of their tunable optical and electronic properties and low-temperature solution processing. NQD research has rapidly evolved from the creation of NQDs with high size- and shape-uniformity and well-defined optical properties to the assembly of NQDs as building blocks into ordered superstructures.<sup>4–7</sup> NQD assemblies are predicted to exhibit novel properties arising from the coherent quantum mechanical interactions of constituent NQDs. In combination, the ability to control the characteristics of individual NQDs as well as the many-body exchange interaction in NQD solids is expected to yield a new type of condensed matter. This is an exciting development for fundamental and applied materials science alike as it enables the creation of materials by design, including material combinations that have heretofore not been possible. In this review article, we aim to capture the vitality stemming from the

<sup>a)</sup>Electronic mail: th358@cornell.edu

opportunity for discoveries of fundamental structure-property relationships and related applications in nanotechnology of NQD-based materials and their assemblies.

The recent worldwide surge of research in renewable energy systems has put an additional spotlight on nanomaterial-enabled energy technologies. Nanomaterials have been heralded as promising components in a broad variety of low-cost, high-performance energy conversion, and storage technologies. Advantageous physical properties of nanomaterials for energy applications include high absorption cross sections, enabling efficient light absorption in thin films, highly efficient light-to-charge conversion mechanisms capable of breaking the Shockley–Queisser limit, and energy levels which can be tuned to achieve multijunction solar cells in low cost configurations.<sup>8</sup> The potential of NQDs as thermoelectric materials derives from the ability to decouple trends in thermal and electrical conductivity.<sup>9–16</sup> Specifically, the nanostructured interfaces in NQD solids should scatter phonons more effectively than electrons and size-dependent quantum confinement enhancement of the thermoelectric power factor is expected.<sup>17</sup> Moreover, the sharp density of electronic states found in strongly confined NQDs presents an optimal electronic structure for thermoelectric materials with theoretical predictions of the thermoelectric figure of merit (ZT) values as high as 10,<sup>17,18</sup> compared to current record materials with ZT  $\sim$  2–3.<sup>19–21</sup> A comprehensive review of nanomaterials in energy technologies is impractical here; several good reviews about the role of nanomaterials in photovoltaic (PV),<sup>22–24</sup> light-emitting diodes (LEDs),<sup>25,26</sup> and thermoelectric,<sup>27</sup> and energy storage<sup>28–30</sup> technologies have been published. Potential applications of NQDs in electronic and memory devices have also been reviewed.<sup>5</sup>

Figure 1 shows a simplified cartoon of a NQD thin film device; the colloidal NQD building blocks are modeled as monodisperse spheres; important details regarding the surface of the NQDs, their shape, and arrangement within the film are neglected. Compared to conventional thin films, two challenges are immediately apparent: First, NQDs within the device structure need to be electronically coupled with each other and with their surrounding contacts. Charge transport, normally constrained by hopping across disconnected particles, is dramatically enhanced at points of physical contact by direct carrier conduction. Secondly, the NQD film has a large void fraction and surface area, demanding robust

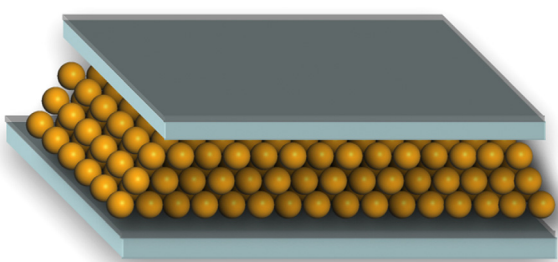


FIG. 1. (Color online) Basic schematic of a NQD thin film device. The NQD building blocks are simplified as monodisperse spheres in a close-packed ordered assembly. The details shape of the crystal core and surface chemistry of the crystal facets are omitted for simplicity.

control over interfacial properties to preserve the intrinsic properties of the NQD. These challenges warrant detailed discussion since they present arguably the most important roadblocks on the path towards NQD-based technologies.

Understanding and controlling the coupling between proximate NQDs in the condensed phase is critical for several reasons. First, from a fundamental perspective, with enhanced coupling between dots, new collective excitonic and vibrational bands should develop; making possible the independent tailoring of electronic and vibrational spectra of the NQD solid. Additionally, to integrate NQDs into device technologies, they must be electronically coupled to each other and their surroundings. Isolated NQDs which do not interact with nearby dot but rather the surrounding environment have been successfully applied as catalysts<sup>31,32</sup> as well as fluorescent biomarkers or drug delivery vehicles.<sup>33,34</sup> By contrast, in solid-state devices, the performance of essentially all proposed NQD-based technology depends critically on efficient interdot electronic coupling. Consider, for example, NQD-based optoelectronic devices; in the case of NQD solar cells, photoexcited carriers must be extracted from the NQDs, whereas in a LED, carriers must be injected into the quantum-confined system where they radiatively recombine.

The high surface area and void fraction of the NQD film present challenges and opportunities for advanced surface science tools in the characterization and processing of NQD thin films. With the approximation of monodisperse hard spheres, the void fraction is approximately 26%. Depending on the shape of the NQD and the symmetry of the assembly, this void fraction can be lower (e.g., in assemblies of space-filling cubes) or higher (e.g., in nonclose-packed assemblies). Clearly, the composition of the void volume has important implications on the electrical and optical properties of the NQD film. Ideally, the “void” matrix can be engineered to participate purposefully in charge transport processes while at the same time preserving the structural and chemical integrity of the NQD matrix interface.

The fraction of atoms near the surface of the NQD and the surface area of the NQD film are very high. For example, in a typical 6 nm diameter NQD, approximately half of the atoms are within one unit cell from the dot surface. The high surface area is particularly important with regards to charge trapping and chemical reactions, which can be either beneficial (e.g., photocatalysis) or detrimental (e.g., oxidation or corrosion). Inorganic-organic interfaces, such as the NQD core/ligand system in the as-synthesized dots, are inherently defective and far more complex than their all-inorganic counterpart. Given the nature and significance of this interface challenge, there are tremendous opportunities to apply knowledge and technologies that have already been developed to resolve similar interfacial obstacles in the microelectronics industry.

As-prepared colloidal NQDs are generally coated with long-chain organic ligands that passivate their surfaces and stabilize the colloidal suspension. A schematic of the colloidal NQD and the surrounding ligand shell, a molecular dynamics (MD) simulation of the NQD/ligand complex, and a high-resolution transmission electron microscopy (HRTEM) image to illustrate the crystallography and faceting of the NQD core

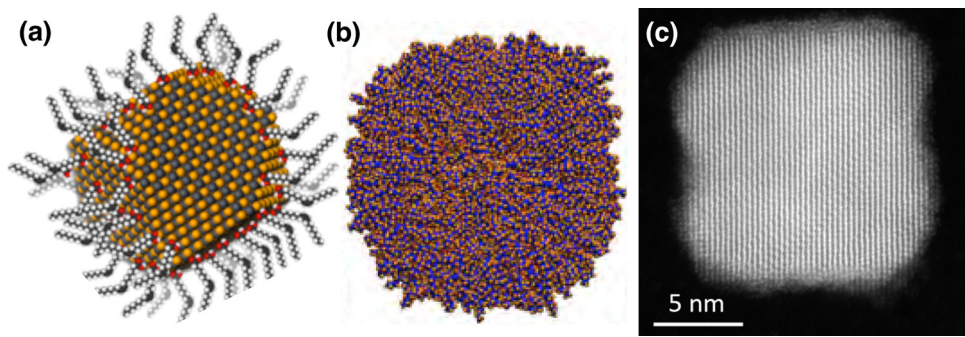


Fig. 2. (Color online) (a) Basic model of colloidal NQD with stabilizing ligands. (b) Detailed molecular dynamics model of NQD with full ligand shell, and (c) high-resolution TEM image showing crystal shape and faceting. [Image credit: W. Baumgardner and L. Fitting-Kourkoutis (unpublished)].

is shown in Fig. 2. The physics and chemistry of the surface bound ligand play critical roles in all stages of the NQD's life ranging from birth, the nucleation in the colloidal solution environment, through youth, the growth rate of specific crystal facets, work, the electronic coupling of the NQD to its surrounding in a functional device, and ultimately death, the degradation of the NQD due to undesirable surface reactions.<sup>35</sup>

On one hand, the ligand shell is critical for stabilization of the colloidal NQDs. Without appropriate surface stabilization, NQDs are prone to sintering into mesoscopic equilibrium aggregates; thus losing their nanoscale size-dependent properties. On the other hand, the ligand shell is electrically insulating and therefore isolates individual NQDs from each other. The presence of organic ligands surrounding the NQD surface therefore presents both a challenging barrier to inter-dot coupling and an opportunity to tune the nature of the artificial bond. Recently, there have been several exciting advances towards resolving this “ligand problem” via chemical and physical treatments of the NQD; we will summarize these advances in Sec. III B of this review.

The focus of this review is NQD solids and their tunable electronic structure in the context of their potential application in optoelectronic devices including PVs and LEDs. In the next section, we describe the conceptual framework and theoretical considerations of NQD solids as artificial solids with tunable optoelectronic properties. In Sec. III, we review recent experimental advances towards NQD solids with experimental control over the (i) energy levels of NQD as artificial atoms, (ii) interdot coupling as artificial bonds, and (iii) structure of the NQD assembly as an artificial crystal. Finally, we discuss outstanding challenges and perspectives of future developments in the field of NQD solids and conclude in Sec. IV.

## II. ARTIFICIAL SOLIDS—CONCEPTUAL FRAMEWORK AND THEORETICAL CONSIDERATIONS

Figure 3 illustrates the conceptual framework of an artificial solid as a crystal of crystals. The choice of the term “artificial” in the description of NQD solids is somewhat unfortunate given that they are certainly real. Artificial in this case refers to the fact that the properties of the solids can be changed by design, so the term “designer crystals” has also been used. The concept is based on analogies between a

classical solid, comprised of atoms, and an artificial solid, comprised of NQDs as artificial atoms. This analogy is helpful in describing the electronic structure of the solid. For example, in both classical and artificial solids, the properties can be described in the language of condensed matter physics as a function of three key parameters: the energy levels of the constituent atoms, the bonding between the atoms, and the structural arrangement of atoms within the solid.<sup>7,36</sup>

Notwithstanding the analogies, there are also two important discrepancies to point out. First, in contrast to indistinguishable atoms, NQDs as artificial atoms are inherently inhomogeneous. With the exception of magic-sized NQD and cluster crystal compounds, like Cd<sub>17</sub>S<sub>4</sub>(SCH<sub>2</sub>CH<sub>2</sub>OH)<sub>26</sub>,<sup>37</sup> even in a relatively homogeneous NQD ensemble, no two NQDs are truly identical due to small experimental variations in size, shape, composition, ligand coverage, etc. Consider, for example, the PbS NQD shown in the high-resolution TEM image in Fig. 2(c); although the ensemble of NQDs can be described by an average shape and size distribution, small variations in the number of atoms in the crystal, surface reconstruction, or number of surface-bound ligand render each NQD unique. This variability among NQDs in the ensemble has important implications on the electronic structure of the assembly, which we discuss in detail below. The second important difference is that in a classical solid, parameters like the electron affinity, the bond length, or crystal symmetry are natural constants. However, in the artificial solid, each of these parameters can

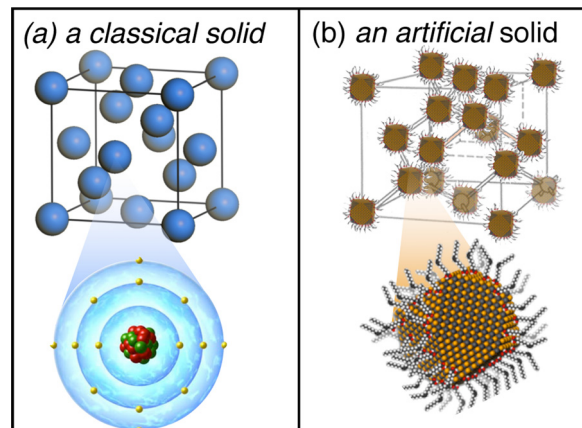


Fig. 3. (Color online) Schematic illustration of (a) classical solid comprised of atoms (i.e., carbon atoms in a diamond lattice) and (b) analogous artificial solid comprised of NQD as artificial atoms.

be independently modified. The prospect of exploiting this tunability to create novel artificial materials with properties by design has created enormous interest among scientists and engineers.<sup>38–41</sup> Thanks to the immense progress made in nanomaterials research in recent years, the new artificial periodic table of nanomaterial building blocks with tunable properties has emerged and continues to grow. The availability of these building blocks and parallel advances in their assembly into ordered superstructures have created unprecedented degrees of experimental freedom to create novel materials. Coherent many-body interactions between similar or dissimilar constituent NQDs are expected to give rise to new physical phenomena. The theoretical considerations underlying the interactions between NQDs in the solid are discussed next.

The electronic structure of artificial solids can be described through direct analogies to the formation of hybridized and extended states in atomic solids (see Fig. 4). We will first review how electronic structure in classical solids evolves from atoms to molecules to solids and then illustrate how analogous concepts describe the evolution of the electronic structure in artificial solids comprised of NQDs.

Isolated atoms are characterized by discrete energy levels that arise from quantum mechanical considerations of the electron orbitals. Energy levels in the simplest atom, hydrogen, are well-described by analytical solutions to the Schrödinger equation. In more complex, multielectron atoms, the Hamiltonian includes the kinetic energy of electrons, the attraction between the electron and the nucleus, and repulsion between electrons. Analytical solutions to the Schrödinger equation for multielectron atoms are not feasible and approximations such as the Hartree–Fock self-consistent field approach are required.<sup>42</sup>

In molecules, quantum mechanical coupling between proximate atoms will split the atomic energy levels. Consider, for example, molecular hydrogen, H<sub>2</sub>. In the language of molecu-

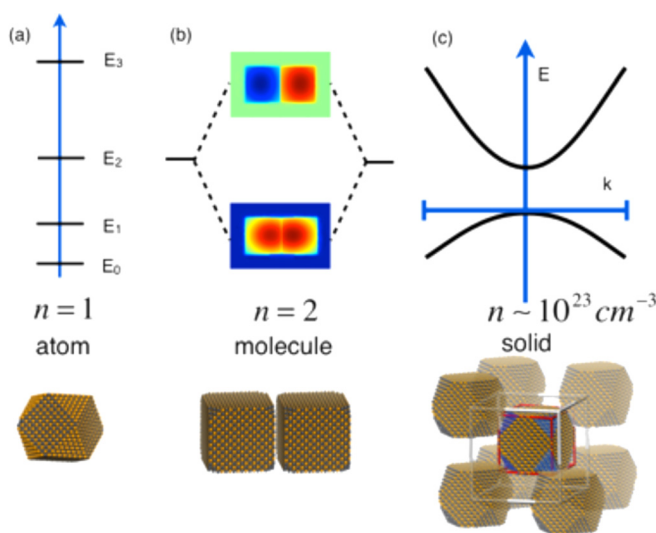


FIG. 4. (Color online) Evolution of the electronic structure from (a) discrete energy levels NQD as artificial atoms to (b) hybridized energy levels in artificial molecules and (c) continuous energy bands in NQD artificial solids. [Energy levels in are based on effective mass calculations by J. Yang and F. Wise (unpublished)].

lar orbital theory,  $n$  atomic orbitals will hybridize to form  $n$  molecular orbitals. This splitting, or hybridization, of atomic states leads to the formation of new states: a symmetric (or bonding) state and an asymmetric (or antibonding) state.

In the condensed phase, coupling between  $n$  atoms leads to  $n$ -fold splitting of the energy levels. The periodic arrangement of atoms in a crystalline solid thus results in the formation of an energy continuum, or a band. Any energy is possible within a certain range or bandwidth of energies and the spectrum of available energies defines the density of states. Within a given band, the energy varies continuously with the wave vector ( $k$ ) as shown in Fig. 4(c). In the case of a semiconductor solid, the filled energy levels (valence band) are separated from the empty energy levels (conduction band) by the energy gap and the population within the bands is described by the Fermi–Dirac distribution.

The evolution of electronic structure from isolated NQDs (as artificial atoms) to extended states in artificial solids parallels the evolution of electronic structure from discrete atomic states to energy bands in atomic solids. As mentioned above, the inhomogeneous nature of NQDs introduces perturbations to the idealized artificial solid structure which in turn lead to interesting physical phenomena.<sup>43</sup> We will first discuss the evolution of the electronic structure in the idealized scenario in which NQDs are assumed identical and then describe how experimental variations in NQD properties perturb the idealized electronic structure. This review will focus predominantly on NQDs that are spatially confined in three dimensions, which are sometimes referred to as 0D systems. There has also been significant progress in the theoretical and experimental investigation of nanostructures confined in one dimension (quantum wire or 1D systems)<sup>44,45</sup> and two dimensions (quantum well or 2D systems).<sup>46–48</sup> The shape of the NQD is often approximated as a sphere or a cube, although the detailed three-dimensional shape depends on the structure of the crystallographic facets as discussed in detail in Sec. III A below.

Colloidal semiconductor NQDs are typically prepared in diameters ranging from 2–10 nm and consist of approximately  $n \sim 10^2$ – $10^5$  atoms; this size range is intermediate to the discrete atomic and extended solid case described above. Here, the density of states formed from the hybridization of  $n$  atomic orbitals is insufficient to form a continuous energy band; instead, the electronic structure of an ideal NQD is defined by the discrete density of electronic states.

The influence of spatial confinement on the electronic structure of NQDs has been discussed since the 1980s in pioneering work by groups of Brus,<sup>49</sup> Henglein,<sup>50</sup> and Efros.<sup>51</sup> Spatial confinement of the charge carriers (electrons and holes) to the volume of the dot influences the energy levels in two important ways. First, the kinetic energy, also known as the confinement energy, increases proportional to  $1/d^2$  for both electrons and holes, where  $d$  is the diameter of the dot. Second, electrostatic energies (Coulombic attraction between electrons and holes and the solvation energy loss) increase as  $1/d$ .<sup>49,52</sup> The simplified effective mass approximation models the NQD boundary as an infinite barrier; this approximation leads to an overestimation of the degree of

quantum confinement. More sophisticated models based on semiempirical pseudopotentials,<sup>53</sup> or tight-binding models,<sup>54</sup> have shown better agreement between experiment and theory.

Although size-dependent energy levels are a general feature of NQDs, the magnitude of the effect depends significantly on the electronic properties of the NQD core composition. For example, quantum confinement effects in Si NQD only become significant in structures with dimensions less than  $\sim 3$  nm.<sup>55</sup> In lead salt NQDs ( $\text{PbX}$ ;  $X = \text{S}, \text{Se}, \text{Te}$ ) on the other hand, quantum confinement effects are much more pronounced, evident even in structures up to 15 nm in diameter.<sup>56</sup> In general, these effects are most pronounced in NQDs of semiconductors with small effective masses and small energy gaps.<sup>49</sup> The magnitude of the shift in energy levels relative to the bulk depends on the dimensions of the nanostructure relative to the characteristic electronic length scale—the Bohr radius of the bound state of the electron or hole.<sup>56</sup> Finally, within a given material, the quantum confinement effects vary for different extrema of the band structure.<sup>57,58</sup>

The relationship between NQD size and energy levels can be readily visualized by basic optical absorbance spectroscopy of NQDs in solution or films. The absorption spectrum in Fig. 5 illustrates an example of discrete optical transitions in PbS NQD. The lowest energy transition is attributed to the formation of an exciton—a bound electron-hole pair in which both carriers have an *s*-like envelope function. Higher-level excitations are also visible and their origin has been investigated with optical spectroscopy<sup>59</sup> and scanning tunneling spectroscopy.<sup>60</sup> The excitonic absorption spectrum thus provides a convenient first-line characterization of the NQD size (given by the absolute energy of the excitonic peak,  $\alpha$ ) and the NQD diameter distribution, (which is related to the width of the excitonic peak,  $\Delta\alpha$ ). The width of the excitonic peak has two components: homogeneous broadening due to inherent exciton-phonon coupling and inhomogeneous broadening arising from the distribution of NQD sizes.<sup>56</sup> Further details concerning the electronic structure of NQDs as a function of their size, shape, composition, and surface chemistry are provided in Sec. III A.

To understand electronic coupling between proximate dots, we need to consider quantum mechanical and electrostatic effects (Fig. 6). As the separation between two neighboring NQDs is reduced, their envelope wave functions can overlap, leading to quantum mechanically coupled dots. The simplified two-dot system shown in Figs. 4(b) and 6 can thus be considered as an artificial molecule. The emerging bonding and antibonding states and their dependence on interdot separation have been investigated in GaAs/AlGaAs artificial molecules using photoluminescence (PL) spectroscopy.<sup>61</sup> Electrons can tunnel between the dots at a rate,  $\Gamma$ , proportional to the coupling energy,  $\beta \sim h\Gamma$ , where  $h$  is Planck's constant. The strength of the coupling depends exponentially on the spatial width ( $\Delta x$ ) and square root of energetic height ( $\Delta E$ ) of the barrier between the artificial atoms. To a first approximation, this dependence can be stated in the exponential expression:<sup>62</sup>

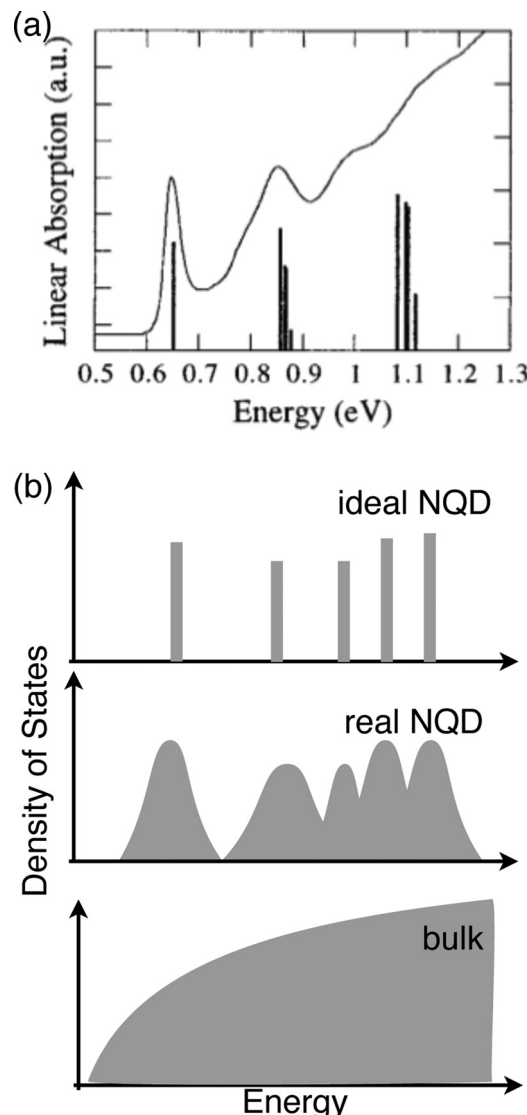


FIG. 5. Quantized electronic states in PbS NQD. (a) Absorption spectrum and calculated transition strengths of 8.5 nm PbS NQDs and (b) density of states in an ideal and real NQD compared to the density of states in a bulk solid. [From F. Wise, Acc. Chem. Res. **33**, 773 (2000).]

$$\beta/h \approx \exp \left[ -2\Delta x \left( \frac{2m^*\Delta E}{\hbar} \right)^{1/2} \right]. \quad (1)$$

This equation illustrates that, to achieve efficient coupling between NQDs, small separation between dots ( $\Delta x$ ) and low barrier height ( $\Delta E$ ) are desired. Experimental progress towards efficient interdot coupling is discussed in Sec. III B.

Electrostatic aspects of interdot coupling arise from the fact that the addition or removal of a charge from a NQD involves a Coulombic energy penalty. As illustrated in Fig. 6(b), this Coulombic charging energy depends on the self-capacitance of the dot, which in turn depends on the shape of the dot and the dielectric environment inside and outside the dot.

Depending on the relative strength of the coupling ( $\beta$ ) and the charging energy ( $E_c$ ), the character of the artificial

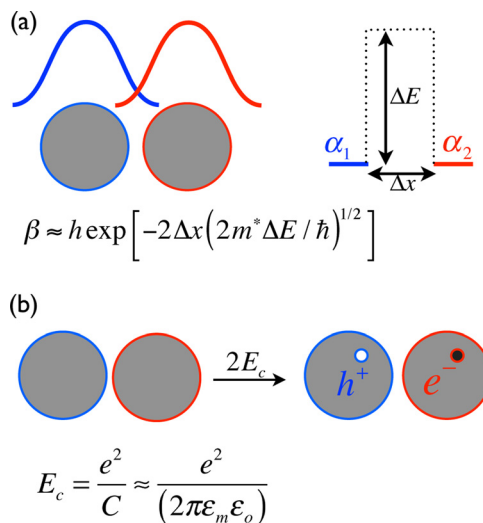


FIG. 6. (Color online) Electronic coupling between proximate NQDs. (a) Quantum mechanical coupling arises from overlap of the envelope wave functions. The coupling energy depends exponentially on the interdot separation and the height of the energy barrier. (b) Electrostatic charging energy ( $E_c$ ) arises from the Coulombic energy penalty to add or remove a charge from the NQD.

bond connecting the NQD can be ionic (with electrons localized on individual dots) or covalent (with electrons delocalized over both dots). With sufficient reduction of the barrier height or width, the coupling,  $\beta$ , between NQDs can be sufficiently strong to overcome the Coulombic penalty. The comparison of  $\beta$  and  $E_c$  therefore defines an important transition in the electronic structure known as the Mott metal-to-insulator transition.<sup>63</sup>

By analogy to classical crystals, coupling between idealized NQD arranged in periodic one-dimensional (1D), 2D, or 3D structures can lead to the formation of extended states (minibands) separated by energy gaps. The number of states within a given miniband corresponds to the number of dots in the crystal while the gap between bands depends on the coupling strength between the dots. In general, the bandwidth is proportional to the coupling energy,  $\beta$ , so that weak coupling yields a narrow band and a large gap and strong coupling will result in wide band and a small gap. Band structures of 2D (Ref. 38) and 3D (Refs. 64–66) ordered QD assemblies have been calculated. Lazarenkova and Balandin analyzed the band structure of an idealized 3D array of semiconductor NQDs using an envelope function approximation and demonstrated that quantized energy levels of coupled NQDs split to form 3D minibands (see Fig. 7).<sup>65</sup> Their model indicated that discrete NQD energy levels split into minibands for interdot separation less than  $\sim 2$  nm. A similar model was later used by Jiang and Green to systematically study the emergence of minibands in Si NQDs in the context of their potential application in photovoltaics.<sup>64</sup> By accounting for anisotropies in the effective mass of the silicon dot, their model showed a reduced energy gap separation and increased degeneracy of the isotropic solution; these aspects are advantageous for efficient broadband absorption in photovoltaic applications. Optical properties of idealized artificial solids created from InAs NQDs in a InGaAs matrix have

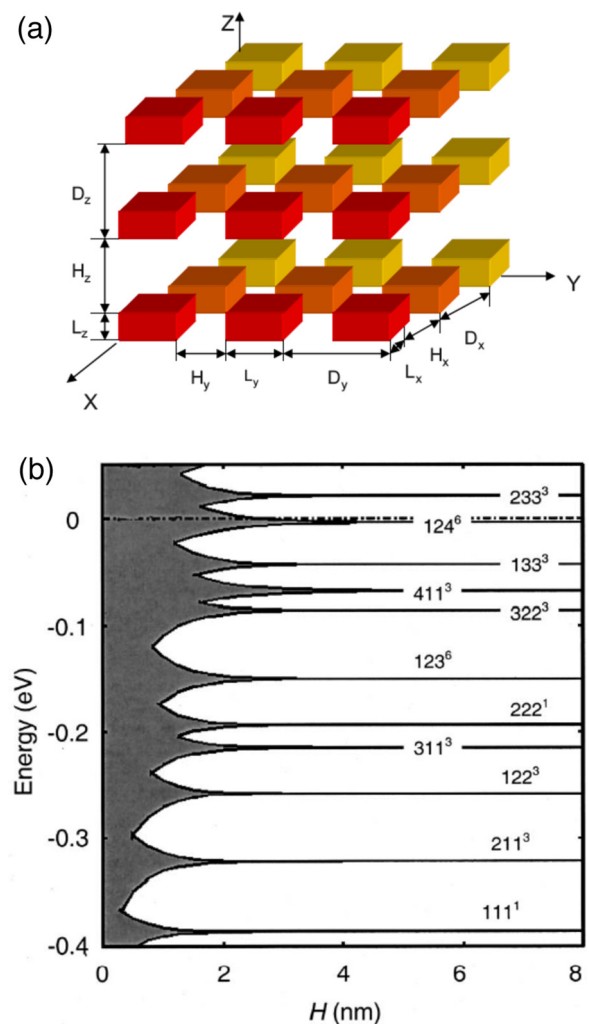


FIG. 7. (Color online) Theoretical analysis of miniband formation in NQD solids. (a) Schematic of the three-dimensionally ordered quantum dot superlattice showing notations for the quantum dot sizes and interdot spacing [from Nika *et al.*, Phys Rev B **76**, 125417 (2007)]. (b) Miniband width as a function of interdot spacing,  $H$  [from O. Lazarenkova and A. Balandin, J. Appl. Phys. **89**, 5509 (2001)].

recently been calculated by Nika *et al.*,<sup>66</sup> their analysis of electron and hole spectra and light absorption predicts that minibands of extended exciton states with high oscillator strength can be formed. A theoretical study of optical nonlinearities in NQD lattices by Takagahara suggests that multipole coupling between NQDs can lead to the creation of a coherent exciton state that extends over many NQDs in the array; the coherent exciton state can collect oscillator strength from many sites, which has a direct impact on the linear and nonlinear optical properties.<sup>67</sup>

Having outlined the basic theoretical considerations of confined and extended states in idealized NQD solids, we now address how the inherent inhomogeneity in *real* experimental NQDs perturb the electronic structure of their assemblies. With current synthesis and separation methods, colloidal NQDs with a relative size distribution of  $\pm 5\%$  are readily achievable. Given the direct relationship between the NQD diameter,  $d$ , and the energy levels,  $\alpha$ , discussed above, this size variation effectively broadens the distribution of

discrete energy levels ( $\Delta\alpha$ ) of the NQDs in the ensemble. As previously mentioned, perturbations to the energy levels of individual NQDs can arise from statistical differences in the composition, the crystallographic faceting, surface chemistry, etc. These aspects are discussed in Sec. III B.

To understand how fluctuations in the discrete energy levels,  $\Delta\alpha$ , influence the electronic structure of the assembly, we need to compare the relative magnitude of the energy level distribution to the coupling strength,  $\beta$ . If the NQDs are identical and strongly coupled (i.e.,  $\beta > E_c$ ) then extended states are formed. However, if the energy level fluctuations,  $\Delta\alpha$ , are larger than the coupling energy, localized states are formed. In this case, the coupling is insufficient to overcome differences in the electronegativity between NQDs in the assembly and charges are effectively trapped on isolated large NQDs. In the case of the artificial two-dot molecule shown in Fig. 6(b),  $\beta < \Delta\alpha$  would be analogous to an ionic bond in which an excited charge would be localized on the larger dot with the higher electron affinity. Oosterkamp *et al.* have demonstrated the transition between ionic and covalent artificial bonds in coupled two-dot (GaAs/AlGaAs) systems.<sup>68</sup> In the extended solid, the transition from localized (i.e.,  $\beta < \Delta\alpha$ ) to delocalized (i.e.,  $\beta > \Delta\alpha$ ) electronic states is known as the Anderson transition, which has been well studied in atomic crystals and more recently in artificial solids.<sup>69,70</sup> Smith and Nozik used pseudopotentials fit to *ab initio* results to theoretically study the electronic structure of a 1D, 2D, and 3D NQD arrays.<sup>71</sup> Their calculations demonstrated that morphological or configurational inhomogeneities significantly influence coupling in the array and that localization of the wave function can occur even in the case of an artificial solid comprised of (identical) NQDs.

Remacle and Levine have pointed out that the electronic structure of NQD solids also contains intermediate transitions in between the extended ( $\beta > \Delta\alpha$ ) and site localized ( $\beta < \Delta\alpha$ ) states.<sup>72</sup> These intermediate, domain-localized, states illustrate the diverse, and importantly tunable, characteristics of the electronic phase diagram of NQD solids. The rich electronic structure of NQD solids can be visualized in a quantum phase diagram as shown in Fig. 8, which illustrates the interplay of the coupling strength ( $\beta/(\beta + E_c)$ ) and the disorder in the NQD solid. The coupling strength can be tuned by adjusting the height and width of the energetic barrier between the dots [see Eq. (1)]; the disorder can be independently tuned by changing, for example, size and shape distribution of the NQD. NQD solids comprised of homogeneous, but weakly coupled dots are characterized by localized states (left hand side). Extended electronic states are formed if the dots are strongly coupled (right hand side), but only if the bandwidth of the resulting miniband is larger than the site dispersion energy ( $\beta > \Delta\alpha$ ). We discuss experimental signatures of delocalized states in Sec. III D.

### III. EXPERIMENTAL PROGRESS TOWARDS ARTIFICIAL SOLIDS

This section discusses recent experimental progress towards NQD solids introduced previously. The organization

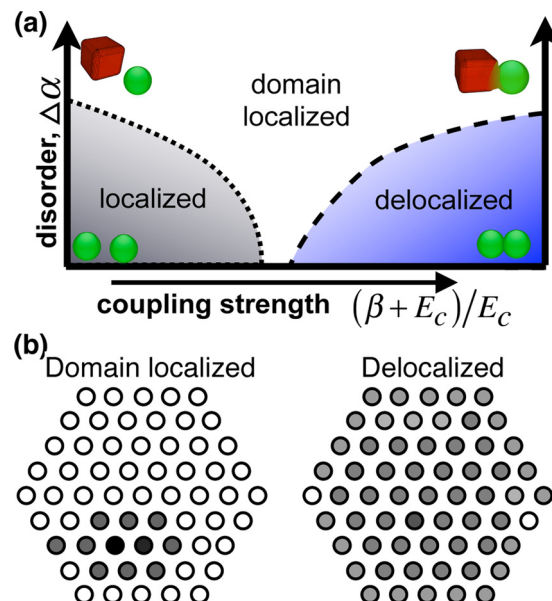


Fig. 8. (Color online) Electronic structure of NQD solids (a) schematic phase diagram of electronic states as a function of coupling strength and disorder (b) illustration of localized and delocalized states in a hexagonal 2D array of NQD [adopted from Remacle and Levine, ChemPhysChem 2, 20 (2001)].

of this section parallels the discussion of theoretical consideration of NQD solids in Sec. II. We will first review experimental aspects of controlling the electronic structure within individual NQDs as a way to tune the properties of the “artificial atom.” Continued progress in colloidal NQD synthesis has enabled remarkable progress in the creation of NQDs with precise control over relative energy level (i.e., tuning the energy gap via quantum confinement) and absolute energy levels (i.e., tuning the electron affinity and ionization potential relative to vacuum). Coupling, both between NQDs and from NQDs to external contacts, is discussed in the framework of adjusting the “artificial bond.” There have been remarkable advances in resolving the “ligand problem” by tailoring of the coupling across the NQD boundary through chemical and physical treatments of the NQD surface. Progress in directing the self-assembly of NQDs into ordered assemblies is reviewed in terms of controlling the structure of the artificial solid. Lastly, we will review how concurrent advances in controlling the artificial atom, artificial bond, and structure of the artificial solid have enabled new fundamental insights and enhanced technological performance of charge transport in NQD solids. We focus in this section primarily on semiconductor NQDs and to a lesser extent on metal particles, which have been reviewed elsewhere.<sup>73</sup>

To put the fundamental experimental challenges in the context of their technological application in thin film devices, Fig. 9 provides a simplified schematic of a NQD-based thin film electronic device. Although the figure illustrates the specific light-to-charge processes of a NQD PV device, the general considerations are similar in LEDs, field effect transistors, or thermoelectric devices. The successful operation of NQD-based devices depends critically on understanding and controlling a number of coupled interfacial

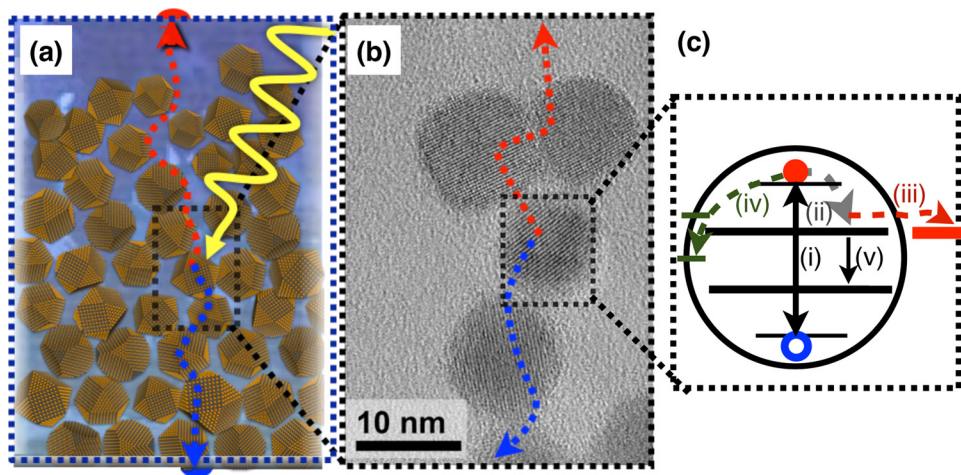


FIG. 9. (Color online) Elementary operating steps in a NQD thin film device. Photoexcitation and charge separation in a NQD solar cell (a) schematic and (b) TEM image of PbSe NQDs. (c) Illustration of subprocesses of photovoltaic cell including (i) photoexcitation, (ii) thermalization of hot carriers to the lowest unoccupied state, (iii) desirable charge transfer across the NQD boundary, (iv) undesirable trapping in surface states, and (v) recombination. Other ultrafast processes, such as hot electron transfer or multiexciton generation are omitted for clarity; these processes are discussed in the text.

subprocesses. In the illustrated example of a NQD solar cell, an incident photon generates an electron-hole pair, or exciton, which must be split at the NQD boundary and transported to their respective external electrodes [Fig. 9(a)]. Controlling energy levels *inside* the NQD is important for tuning the wavelength of absorbed or emitted light. Likewise, the electronic landscape *outside* the dot must be tailored to facilitate charge separation (in the case of a PV device) or charge injection (in the case of a LED). In the specific example of NQD-based solar cells, the charge transport through the film must be engineered to avoid charge trapping, which is particularly critical in light of the high interface density within the NQD film.<sup>74</sup> The kinetics of the subprocesses of separation and transport across the various interfaces must surpass competing recombination and trapping dynamics. Specifically, in a high-performance NQD solar cell, photogenerated carriers must be extracted at a rate faster than the trapping and recombination rates [see Fig. 9(c)].

Processes such as hot electron transfer or multiexciton generation (MEG) are omitted from Fig. 9(c) for simplicity, but these processes have generated significant interest so a brief discussion is warranted. Hot electron transfer refers to the extraction of photoexcited carriers from the NQD before they relax to a ground state; Tisdale *et al.*<sup>75</sup> have recently observed this process in time-resolved second harmonic generation measurements of electron transfer from PbSe NQD to titanium oxide acceptors. In MEG, a photon with energy several times the energy gap of a NQD is converted to multiple electron-hole pairs. The first, clearest, and most dramatic observations of MEG were all obtained with lead-salt NQDs.<sup>76,77</sup> The strength of the MEG process is the subject of much current debate and even controversy.<sup>78–85</sup> Reports on photocurrents from PbS QD to TiO<sub>2</sub> in a sensitized PV structure,<sup>86</sup> and more recently PbSe NQD thin film solar cells,<sup>87</sup> with quantum yield greater than one electron per photon, have intrigued the community and underscored the

promising potential of NQD-based solar cells with conversion efficiencies beyond the Shockley–Queisser limit.<sup>8</sup>

Charge transfer kinetics are fundamentally related to the energy level offsets via Marcus theory,<sup>88</sup> however, whether Marcus theory appropriately describes charge transfer among NQDs remains to be validated and apparent contradictions exist.<sup>89</sup> Furthermore, the active layer must be structured, across multiple length scales, to provide a bicontinuous transport pathway for each charge to their respective electrode. Lastly, each of these criteria must be realized in a scalable, robust, and low-cost device platform. Clearly, the list of constraints and requirements for the successful operation of NQD devices is daunting; however, a commonality of these challenges is their critical dependence on the physical and chemical nature of the NQD interface. Below, we review some of the recent progress towards resolving these challenges.

Among the various colloidal NQD materials currently under investigation, group IV-VI and II-VI compound semiconductors stand out as fundamentally intriguing and experimentally advantageous artificial atoms for the study of NQD solids for several reasons: First, strong quantum confinement effects enable broad tunability of the NQD energy levels. PbX NQDs in particular are among the most strongly quantum-confined systems. Thanks to the large Bohr diameter of the exciton (46 nm in PbSe),<sup>50,56</sup> adjusting the NQD diameter between 2 and 10 nm provides experimental control to prepare materials with a tunable energy gap ranging from 0.4 to nearly 2 eV.<sup>90–94</sup> Due to the low effective mass of electrons and holes in PbX NQDs, the envelope wave functions extend significantly outside the boundary of the dot and enables efficient interdot quantum coupling. The nearly equivalent effective mass of electrons and holes in PbX simplifies the theoretical interpretation of coupled electronic states.<sup>56</sup> In contrast, most V-III and many II-VI semiconductors are characterized by dissimilar effective masses; in these materials, the *p*-like valence band character produces a

complicated spectrum under confinement and makes signatures of extended states more difficult to interpret.<sup>66</sup>

### A. NQD building blocks—tuning artificial atoms

The availability of NQD building blocks with well defined size, shape, composition, doping, and surface chemistry is arguably the most critical prerequisite for fundamental studies and technological applications of NQD solids. Tuning the electronic structure of the NQD presents a very versatile degree of freedom in the creation of artificial atoms with properties by design. The earliest quantum dot and quantum well structures have been prepared by vacuum-based techniques whereby semiconductor structures were grown, bottom-up, on planar support substrates. The geometry of the quantum structure is a function of kinetic and thermodynamic considerations of the growth conditions, including growth rate, temperature, and lattice mismatch between the grown material and the substrate; these parameters define four growth modes including the Frank van der Merwe growth of conformal films (i.e., 2D quantum wells), Stranski–Krastanov, Volmer–Weber, and self-organized quantum dot growth.<sup>95</sup> Early work on these vapor phase methods has demonstrated the growth of a variety of quantum-confined semiconductor heterostructures including Ge/Si,<sup>96–98</sup> InGaAs/GaAs,<sup>99,100</sup> InP/GaInP,<sup>101</sup> and InP/AlGaAs.<sup>102</sup>

To expand the control over composition and geometry of quantum-confined nanostructures, nonvacuum based synthesis methods were investigated. Starting in the early 90s, several solution based quantum dot synthesis methods began to emerge. The hot-injection method pioneered by Murray<sup>4,103</sup> is arguably the most versatile and well-studied approach and will be the focus of the discussion below. Although the vacuum based methods are much “cleaner” than the solution-based synthesis, the versatility of the chemical interactions between solvent, ligand and precursor introduces synthetic degrees of freedom for the creation of NQDs with varying size, shape, and composition. Intensive research efforts have demonstrated that these interactions can be exploited in various synthesis approaches in organic and aqueous environments including heating-up,<sup>104</sup> inverse micelle methods,<sup>105</sup> as well as gas phase reactions<sup>106</sup> and supercritical fluid approaches.<sup>107</sup> NQDs have also been prepared in solid matrices; for example, in glass,<sup>108</sup> although the control over shape and size is not as refined as for the solution-based approaches. The mechanism governing the growth of colloidal NQDs is fundamentally different from the Stranski–Krastanov growth of quantum dots in vacuum-based approaches discussed above. A comprehensive review of NQD synthesis techniques is not practical here; thorough reviews are available in the literature.<sup>35,109</sup>

Figure 10 shows the essential steps of the colloidal NQD synthesis in the illustrative example of PbSe NQDs. In contrast to vacuum-based methods, the colloidal NQD synthesis is performed via inexpensive solution-based techniques using a Schlenk-line setup to create an air-free reaction environment [Fig. 10(a)]. Fundamental NQD synthesis aspects, in particular, the need to independently control the crystal

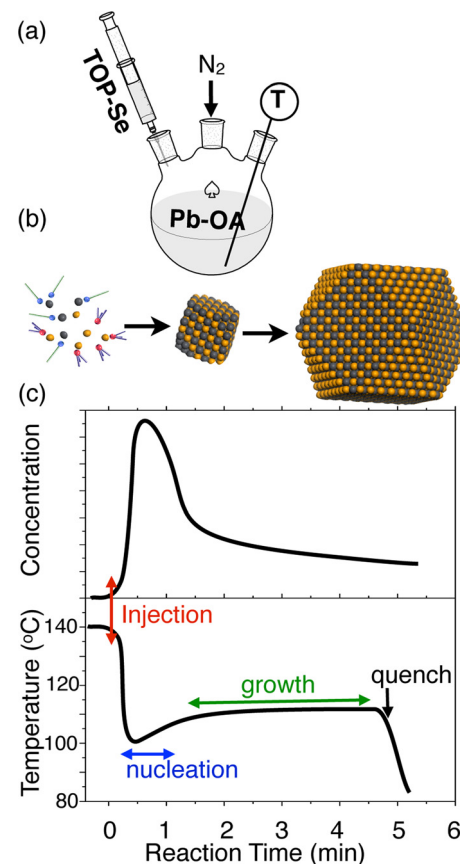


FIG. 10. (Color online) Colloidal NQD synthesis (a) basic wet synthesis experimental setup, (b) conversion of molecular precursors to nanocrystal nuclei and fully developed nanocrystals, and (c) typical concentration and temperature profiles illustrating the temporal separation of nucleation and growth.

nucleation and growth, build on earlier studies of colloid synthesis by La Mer and Dinegar.<sup>110</sup> Classical nucleation theory captures the elementary kinetic and thermodynamic aspects of colloidal NQD nucleation. The free energy change ( $\Delta G$ ) associated with nucleation is governed by the balance between the energetic driving force ( $\Delta\mu$ , the chemical potential associated with the conversion of molecular precursors, or monomers to a crystalline solid) and the energetic penalty for creating a particle/solution interface with surface energy,  $\gamma$ . The driving force for nucleation is conveniently described in terms of the supersaturation,  $S$ , which is defined as the ratio of monomer concentration to the equilibrium solubility of the precursor. With the approximation of a spherical particle, the free energy change is expressed by

$$\Delta G = (4/3)\pi r^3(\Delta\mu) + 4\pi r^2(\gamma), \quad (2)$$

where  $r$  is the radius of the nucleus. This expression predicts the existence of a critical nucleus size,  $r_c = 2\gamma v/(k_B T \ln S)$  at  $d\Delta G/dr = 0$ , which must form for energetically favorable nucleation, where  $v$  is the molecular volume of the NQD material,  $k_B$  is the Boltzmann constant and  $T$  is temperature. Importantly, both the critical nucleus size ( $r_c$ ) and the nucleation rate vary with the degree of supersaturation during the synthesis.<sup>111</sup>

Experimentally, the separation of nucleation and growth in the colloidal NQD synthesis is achieved by rapidly injecting the precursor solution into the colloidal growth environment. As shown in Fig. 10, the injection leads to a rapid spike in precursor concentration and temporary drop of the overall reaction solution temperature. The initial burst of nucleation is thereby temporally separated from the subsequent growth phase. Once the concentration of available precursors is depleted, the particles may continue to grow either by addition of remaining precursors to the growing crystal or by Ostwald ripening—a process in which smaller particles (with higher surface energy) are dissolved in favor of forming larger particles. Depending on the growth mode, the distribution of particle sizes in the reaction solution may either broaden (during early stages of the synthesis) or narrow (during later stages).<sup>109</sup>

In the specific example of II-VI or IV-VI compound semiconductors (e.g., cadmium or lead chalcogenides, CdX or PbX), the NQD synthesis is typically achieved by injecting a chalcogen precursor (e.g., Se-trioctylphosphine, TOP-Se) into a heated solution containing a preheated Cd or Pb precursor, typically in the form of an oleate. Following the initial burst of nucleation, the particles are allowed to grow in the reaction environment for a specified growth period before the reaction is quenched by reducing the temperature or injecting an inert component. The average diameter of the NQDs in the product can be tuned by adjusting basic synthesis parameters including growth time, growth temperature and precursor concentration. Longer growth times naturally lead to larger particles. Higher synthesis temperature leads to a faster growth rate but also increases the nucleation rate. The initial density of nuclei can be adjusted by controlling the ratio of precursor to surface bound ligands,<sup>112</sup> or the composition of the ligand.<sup>113</sup>

Although, the basic nucleation and growth model<sup>110</sup> describes the elementary processes underlying the colloidal NQD formation and has been used to guide much of the size-controlled synthesis advances, the basic model fails to capture the sensitive relationship between NQD growth and the molecular interactions between ligands and solvents or the crystallographic detail of the NQD facets. For example, the concept of distinct and sequential nucleation, ripening, and growth phases discussed above is an unrealistic idealization; more likely case is that these events occur concurrently. The Hens group recently combined experiment and simulation to study the evolution of the supersaturation through the course of the hot-injection synthesis;<sup>114</sup> their results suggest that Ostwald ripening and nucleation occur in parallel since the supersaturation and hence the critical radius decrease during the course of the reaction.

The initial NQD nucleation does not just involve the formation of a spherical nucleus with critical radius,  $r_c$ , as assumed above, but instead appears to go through a number of discrete, magic-sized clusters. Such magic-sized clusters are known from previous studies of metal nanoparticles.<sup>115</sup> Several groups have reported the synthesis of CdX magic-sized NQD and have recently been reviewed by Yu.<sup>37</sup> In the case of lead salt NQDs, Krauss and co-workers have

reported the creation of magic sized PbSe NQDs via a low-temperature synthesis route.<sup>116</sup> Much of the improved understanding of NQD nucleation and growth was enabled thanks to parallel advances in nanomaterial characterization techniques, in particular *in situ* transmission electron microscopy. For example, Zheng *et al.* recently demonstrated how *in situ* HRTEM can be used to probe initial stages of metal particle nucleation and discovered complex growth trajectories including basic growth by monomer addition and particle coalescence.<sup>117</sup>

The approximation of the colloidal NQD core shape as a spherical particle with radius,  $r$ , is an oversimplification since it does not capture the underlying relationship between crystal faceting and the true 3D shape of the NQD. Differences in the physical and chemical nature of specific crystal facets lead to variations in growth rate and these effects have been exploited to tune the shape of the particle. Beyond the impact on the NQD shape, the crystal faceting also has important implications on magnetic, optical, electronic, mechanical, and self-assembly properties of the NQD; these aspects are discussed in a recent review by Polatz.<sup>118</sup> In the case of CdSe NQDs, Alivisatos and co-workers demonstrated a variety of NQD shapes including rods, arrows, and tetrapods.<sup>6,119</sup> For PbSe NQDs, the particle shape evolves from quasispherical to cubic with increasing NQD diameter.<sup>92</sup>

Important details regarding the delicate and often surprising role of molecular interactions between ligands, solvents, and unintentional contaminants on NQD synthesis continue to emerge. For example, Buhro and coworkers revealed that impurities in trioctylphosphine oxide, a commonly used solvent in NQD synthesis, significantly influences the shape of CdSe nanocrystals.<sup>120</sup> Houtepen *et al.* showed that small amounts of acetate, resulting from insufficient drying of the reaction mixture, significantly influences PbSe NQD shape and size [see Fig. 12(a)].<sup>121</sup> Cho *et al.* demonstrated that an impressive variation in shape of PbSe nanocrystals can be achieved by tailoring the key reaction conditions including the nature of the stabilizing agent and solvent as well as the temperature profile of the reaction. The growth of complex nanocrystal geometries, including various shaped wires and rings was attributed to dipole-mediated alignment [see Fig. 12(b)].<sup>122</sup> More recently, Weller and co-workers demonstrate how similarly oriented attachment can be controlled to achieve the transformation of colloidal NQDs into ultrathin, 2D PbS sheets.<sup>47</sup> The improved molecular level understanding of the role of stabilizing ligand and solvent has also enabled the growth of nanocrystals with complex 3D shapes; the most prominent examples are branched nanocrystal tetrapods which have been observed in several materials including CdX (Refs. 122 and 123) and ZnX.<sup>124,125</sup>

It is important to recognize that, even at room temperature, the ligand bound to the NQD surface constitute a dynamic system in which ligands are constantly absorbing/desorbing and exchanging from the NQD surface. These dynamics were recently illustrated in experiments by Hens and co-workers who used transfer nuclear Overhauser effect measurements to characterize the dynamics of carboxylic acid ligand bound to the surface of CdSe NQD.<sup>126,127</sup>

The ability to create NQDs with tunable dimensions and shapes translates into direct experimental control over the energy gap of the NQD. Size-tunable energy gaps are arguably the most attractive feature of semiconductor NQDs and have been demonstrated in a broad range of material systems. As illustrated in Fig. 11 the energy gap of CdSe NQDs can be tuned, spanning the visible part of the spectrum from 3 eV (1.7 nm diameter) to 1.7 eV (15 nm diameter),<sup>4,103</sup> while corresponding lead salt NQDs with diameters ranging from 2 to 10 nm span the range from 2 to 0.4 eV.<sup>90–94</sup> Insights on shape dependent electronic structure and optical properties (i.e., comparing 0 D dots to 1 D rods) continue to emerge in parallel with advances in the controlled synthesis of anisotropic structures of controlled aspect ratios.<sup>128–130</sup>

Beyond the size and shape tunability of single component NQDs, there has been remarkable progress in the synthesis of multicomponent NQD heterostructures ranging from basic spherical core/shell structures,<sup>131</sup> to complex multilayered systems<sup>132</sup> and multicomponent dot/rod structures.<sup>133</sup> Manna and co-workers recently reviewed the synthesis, properties and proposed applications of NQD heterostructures.<sup>134</sup> The precise control over NQD composition affords new experimental degrees of freedom to create NQDs with rationally designed electronic structures. By exploiting differences in the size- and composition-dependent electron affinity and ionization potential, scientists can create structures in which the quantum confinement of electrons and holes can be independently tailored. NQD heterostructures are commonly categorized by adopting the nomenclature of bulk semiconductor heterojunctions. Depending on the alignment of the bulk valence and conduction band levels, the heterojunctions can be either type I (straddling the energy gap) or type II (staggered energy gap). Although this classification is helpful in describing analogous NQD heterostructures, it should be borne in mind that; in contrast to the energy band alignment in bulk systems, the electronic structure of the NQD

heterostructure is characterized by the relative alignment of quantum-confined discrete states.

Access to complex NQD heterostructures has enabled may new insights into quantum-confined electronic structures. Depending on the energy level alignment of at the interface, type I NQD heterostructures can be created to selectively confine the electron, hole, or both wave functions to the core of the particle. An elegant example of the benefits of wave function engineering inside core/shell structures, Pandey and Guyot-Sionnest demonstrated slow electron cooling in colloidal NQDs.<sup>132</sup> They created multicomponent CdSe/ZnS/ZnSe/CdSe core/shell structures shown in Fig. 12(c) to tailor the quantum confinement to reduce both the coupling between electron and hole wave functions as well as reduce the interaction with intermediate traps states and molecular vibrations. By using these sophisticated core/shell structures, they demonstrated the “phonon bottleneck effect”—the decoupling between electronic states and lattice vibrations.

Similar wave function engineering concepts have also been demonstrated in dot/rod heterostructures in which carriers are confined in different dimensions. Depending on the energy level alignment for electrons and holes at the heterojunction, intriguing nanostructures can be created in which one carrier is 3D in the dot while the complementary carrier is delocalized along the rod and thus only confined in 2D. Type II heterostructures have been subject to increased interest due to their potential application in PV and optoelectronic devices. For example, Scholes and co-workers probed photoinduced charge separation in CdSe/CdTe type II heterostructures and found that the relative alignment of the CdSe/CdTe interface can be exploited to tune the energy and lifetime of the charge transfer PL-band.<sup>135</sup> CdSe/CdS heterojunctions [shown in Fig. 12(d)] have been demonstrated as an experimental platform in the study of the quantum-confined Stark effect, which has potential application in optoelectronic switches.<sup>136</sup>

Aside from the above-mentioned effects of the inorganic NQD size and composition on quantum-confined wave function, the physiochemical properties of the NQD surface have a pronounced impact on the electronic structure and carrier dynamics. Arguably, the surface effects are much less understood and controlled than the core effects; this is in part due to the experimental difficulties associated with creating a detailed understanding of the surface structure and in part due to the fact that the surface is dynamic, changing as the NQD interacts with its surrounding environment. A recent paper by Klimov and co-workers on the effect of air exposure on surface properties, electronic structure, and carrier relaxation in PbSe NQDs provides an illustrative example.<sup>137</sup> Their results illustrate the rapid oxidation of the NQD surface to form PbO, SeO<sub>2</sub>, and PbSeO<sub>3</sub>. PL quenching at short oxygen exposure was attributed to enhanced carrier trapping by oxygen absorbed onto the NQD surface. Recovery of the PL after prolonged air exposure was interpreted as a sign of reduced the efficiency of nonradiative recombination channels. Surface chemistry effects have also been carefully considered in recent studies of MEG in NQDs.<sup>81</sup>

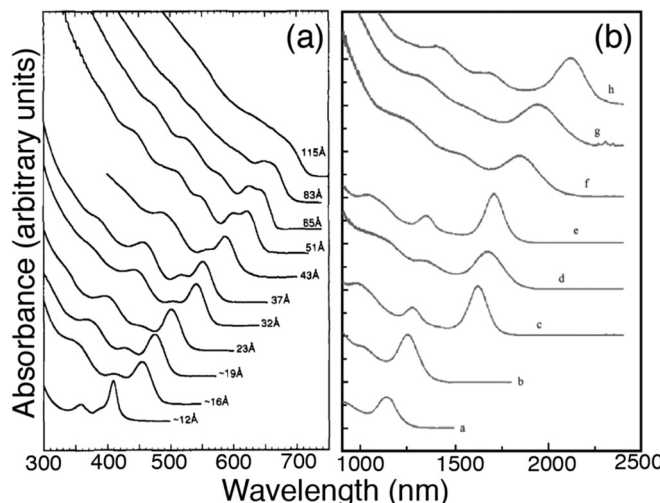


FIG. 11. Size-tunable energy gap. Room temperature optical absorption spectra of (a) CdSe NQD ranging in size from 1.2 to 11.5 nm [from Murray *et al.*, J. Am. Chem. Soc. **115**, 8706 (1993)] and (b) PbSe NQD ranging in size from 3 to 9 nm [from Murray *et al.*, IBM J. Res. Dev. **45**, 47 (2001)].

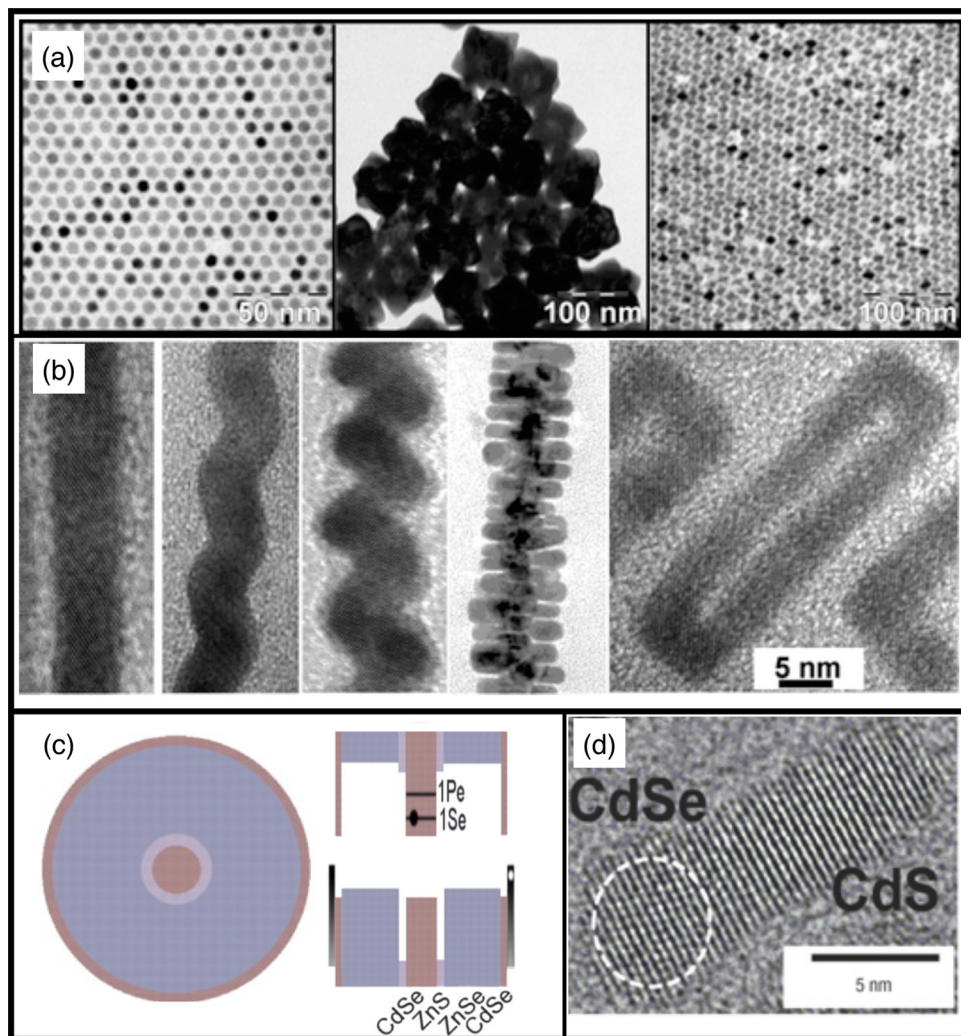


FIG. 12. (Color online) Structural diversity of colloidal semiconductor NQD (a) PbSe NQD shaped as spheres, octahedral and stars [from Houtepen *et al.*, J. Am. Chem. Soc. **128**, 6792 (2006)]. (b) 1D PbSe nanocrystals formed by dipole-mediated alignment [from Cho *et al.*, J. Am. Chem. Soc. **127**, 7140 (2005)]. (c) Multicomponent core/shell structure [Pandey and Guyot-Sionnest, Science **322**, 929 (2008)] and (d) 1D CdSe/CdS heterostructured [from Becker *et al.*, Nat. Mater. **5**, 777 (2006)].

Alignment of the absolute NQD energy level with respect to a standard potential is critical for many processes, in particular, injection or extraction of charge into or out of the NQD to an external contact. Unfortunately, compared to the impressive progress in tailoring the electronic structure within the NQD, understanding and controlling the absolute energy level has remained a challenge. The discrepancy can be attributed in part to experimental difficulties associated with the accurate measurement of absolute NQD energy levels. While relative energy levels; for example, size-dependent energy gaps, can be readily determined using optical techniques such as absorption or luminescence spectroscopy, reliable measurements of the absolute electron affinity or ionization potential has been more elusive.

Common techniques for measuring the size-dependent electron affinity and ionization potential include cyclic voltammetry (CV)<sup>138–139</sup> and photoelectron spectroscopy.<sup>143</sup> Unfortunately, experimental artifacts often obscure the accurate determination of energy levels. In the case of photoelectron spectroscopy, charging of the particle relative to the

substrate requires special consideration;<sup>140</sup> CV measurements are complicated by parallel electrochemical processes that often degrade the NQDs during measurement. Despite these concerns, absolute energy levels determined by CV and photoelectron spectroscopy methods agree reasonably well and are further corroborated by PV device measurements discussed below. The absolute energy levels are sensitive to the chemical and physical nature of the NQD surface. Several scientists have attempted to exploit the sensitivity to tune the absolute energy levels. Ellis and co-workers demonstrated control of the electronic properties of planar, bulk semiconductor surfaces through the interfacial dipoles of attached molecules.<sup>144</sup> In the case of colloidal NQDs, Soreni-Harari *et al.* showed that absolute energy levels of InAs NQDs can be changed by adjusting the linking group and polarity of surface bound ligands.<sup>145</sup>

Size-tunable energy levels provide a valuable experimental degree of freedom in the study of interfacial charge transfer processes underlying the operation of NQD-based PVs. The Kamat group applied size- and shape-control to tune the

photoresponse of CdSe-TiO<sub>2</sub> PV structures.<sup>146</sup> Size-tuned ionization energy and electron affinity have proven beneficial in the work by Choi *et al.* who demonstrated the trend between the PbSe NQD heterojunction energy level offset and the photovoltaic device performance (see Fig. 13).<sup>138</sup> Similar interface energy level offset tuning was also instrumental in the recent discovery of hot electron transfer by Tisdale *et al.*<sup>75</sup> More recently, size-tuned energy gaps have also been critical in the demonstration of NQD-based quantum funnels<sup>147,148</sup> and tandem cells.<sup>149,150</sup> Collectively, these examples illustrate the versatile benefit of programmable energy gaps and interfacial energy level offsets in fundamental studies and NQD-based technologies alike. In NQD-PV in particular, tunable energy gaps facilitate the harvesting of broad-band solar emission. Following the photo-excitation within the NQD as the artificial atom, the generated carriers have to be transported across neighboring NQDs and to external contacts, these processes are governed by interdot coupling along the “artificial bond” as discussed in Sec. III B.

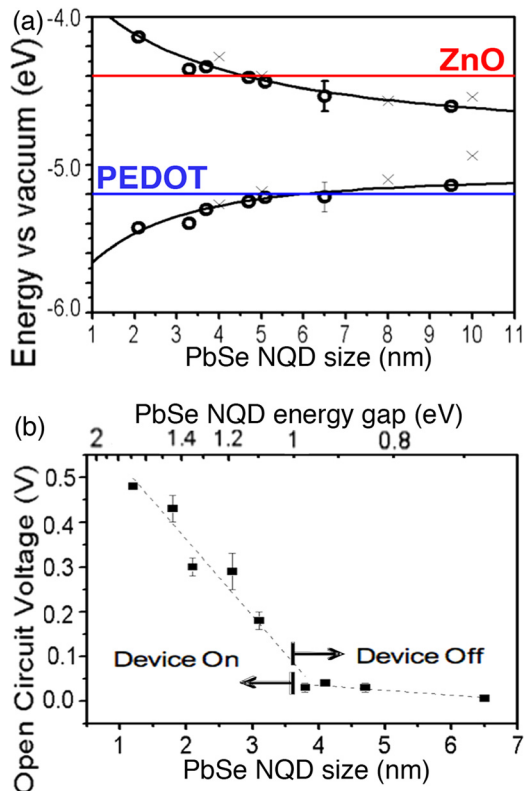


FIG. 13. (Color online) Size-tuned energy level offsets in NQD solar cells. (a) Colloidal NQD synthesis (a) PbSe NQD energy levels measured by CV (black dots). Measured energy levels show good agreement with theoretical calculation. The red line (top) shows the electron affinity of ZnO and the blue line (bottom) shows ionization potential of the hole conductor PEDOT:PSS. (b) Open circuit voltages from devices ( $V_{oc}$ ) with various PbSe NC sizes. Two distinctive domains are observed. Devices made from large ( $d > \sim 3.8$  nm) NCs show no appreciable photovoltaic effect whereas devices made from small ( $d < \sim 3.8$  nm) NCs show increasing  $V_{oc}$  with decreasing NC size. The critical diameter ( $\sim 4$  nm), which defines the transition between the “linear” and “off” domains, agrees reasonably with the CV result. The linear fits (dotted lines) to the respective domains provide information on the minimum interfacial energy level offset required for charge separation PbSe NQD-PV. [From Choi *et al.*, Nano Lett. 9, 3749 (2009)].

## B. Interdot coupling—tuning artificial bonds

In the context of NQD assemblies as artificial solids, the coupling between proximate dots takes the role of the “artificial bond.” Just as in atomic solids, the nature of the artificial bond has profound implications on the properties of the solid. Consider, as an illustrative analogy, the relationship between physiochemical properties of carbon allotropes and their bonding structure. In contrast to the insulating, transparent and hard  $sp^3$  bonded carbon in diamond,  $sp^2$  bonded graphite is conducting, opaque, and brittle. Similar structure-property relationships are anticipated in artificial solids and, importantly, the properties can be rationally tuned depending on the nature of the artificial bond. Here, we discuss coupling between NQD in the solid in the familiar language of chemical bonds. For example, we can describe the interactions between proximate dots by the ionic or covalent character of the “artificial bond.”<sup>151</sup> Coulombic interactions lead to ionic coupling; this principle has also been used to explain physical interactions governing the assembly of binary superlattices of dissimilar NQDs.<sup>152</sup> Covalent artificial bonds; on the other hand, form when the barrier width between particles is sufficiently small to permit significant wave function overlap. The relationship between interdot bonding and transport characteristics and technological applications of NQD solids is discussed in detail in Sec. III D.

In discussing experimental aspects of the artificial bond, it is important to keep in mind that the interstitial medium through which proximate NQDs are coupled is much more complex than a single bond. The interstitial medium itself is comprised of a combination of molecules bound to the NQD surface (e.g., either passivating the surface or connecting neighboring dots), remnant solvent molecules, or a functionalized interstitial organic or inorganic matrix. On one hand, the complexity of the artificial bond introduces new challenges, which must be overcome to understand and predict the interdot coupling; on the other hand, the complexity also introduces versatility and opportunities to engineer the interdot coupling for a particular application. We discuss key challenges and recent progress towards controlled interdot coupling as well as future prospects afforded by the application of advanced surface science techniques. Experimental techniques towards changing the height or width of the interdot barrier can be classified as chemical methods, i.e., by tailoring the chemical moiety in the interstitial of the NQD solid, or physical methods, e.g., thermal annealing or high-pressure treatment. Moreover, we will distinguish between coupling in homogeneous systems (i.e., from dot-to-dot) and coupling in heterogeneous systems (i.e., coupling between dissimilar dots or coupling among nanostructures with different dimensions such as dot-to-wire or dot-to-plane).

The ligand problem introduced in Section II illustrated the challenges associated with balancing the stabilization of the NQD with the need to achieve efficient electronic coupling across the NQD boundary. Long alkyl chains provide colloidal stabilization and passivated the NQD surface, but present a detrimental barrier for interdot coupling. In the condensed phase, the presence of long chain ligands on the

NQD surface generally results in a surface-to-surface spacing of greater than 2 nm. In the case of oleic acid passivated PbS NQD, Shevchenko and co-workers showed that the interdot spacing depends on the structure of the NQD solid; the spacing in faceted 3D NQD solid crystals was ~25% smaller than in NQD films formed by solvent evaporation.<sup>153</sup> The wide barrier created by the ligand shell effectively localizes the wave function within individual NQDs resulting in negligible overlap between electronic wave functions across the dots. Chemical approaches to resolve this challenge rely on the replacement of the insulating ligand with shorter molecules to facilitate interdot coupling. Below, we outline five considerations for chemical approaches used to replace the insulating ligand with a functional linker to couple proximate NQDs and discuss recent examples.

Figure 14 schematically illustrates key aspects of the relationship between NQD surface chemistry and interdot coupling. First, the length of the spacer dictates the width of the interdot barriers, which is exponentially related to the coupling energy as illustrated in Eq. (1). Second the functionality of the surface bound species distinguishes basic ligands (which can only bind to the NQD through one functional group) from bifunctional molecules that can “cross-link” neighboring dots. The third consideration is the chemical nature of the anchor group through which the molecule binds to the surface of the NQD. The type of anchor group governs where and how densely the linker molecule attaches to the particle surface but also influences the electronic structure of the NQD itself. Fourth, the symmetry of the linker molecule influences the nature of the interdot coupling, that is, the use of asymmetric versus symmetric linker molecules may introduce a directionality to charge transfer processes between dots. We note that different anchor groups may exhibit selective affinity to bind to specific NQD facets; this would enable interdot coupling across selected facets; however, the binding affinity to specific facets with asymmetric linkers has yet to be demonstrated. The fifth consideration is the chemical nature of the linker molecule itself. Here we distinguish between linkers that are actively involved in the interdot coupling from inert spacers. The electronic structure of the spacer can be

tuned to have energy levels that are resonant with the quantum-confined energy levels of the NQD, e.g., by choosing either aromatic or aliphatic spacers or including electron donating or withdrawing groups on the spacer. These aspects have been studied in detail in the context of single molecule electronics;<sup>154</sup> insights from the single-molecule studies provide important guidance for future work in controlling the coupling between NQDs. The rich variety of readily available linker molecules introduces the opportunity to precisely fine tune interdot electronic coupling.

There has been significant progress in controlling and understanding the interdot coupling in semiconductor NQD films; we discuss several examples below. In one of the earliest examples of using short linker molecules to enhance interdot coupling in NQD solids, Guyot-Sionnest and co-workers showed that exchanging trioctylphosphine oxide ligands on the surface of CdSe NQDs with 1,4-phenylenediamine increases the conductivity by three orders of magnitude.<sup>155</sup> In the case of lead salt NQD films, Talapin and Murray showed that hydrazine treatment of PbSe NQD films removed the oleic acid ligand and decrease inter-NQD surface-to-surface spacing from 1.1 to 0.3 nm. This reduction of the artificial bond length led to higher quantum exchange coupling and increased the conductance through the NQD array by ten orders of magnitude.<sup>156</sup> These early studies demonstrated the dramatic effect of reduced interdot separation on electronic coupling, but also underscored that chemical treatments of the NQD surface can profoundly influence their electronic structure. For example, in the case of hydrazine treated PbSe NQD films, vacuum treatment changed the transport characteristics from *n*-type to ambipolar and finally *p*-type; the *n*-type character can be restored by re-exposing the PbSe NQD film to hydrazine.<sup>156</sup> The effect of hydrazine treatment on absolute energy levels of PbSe NQD was also illustrated in the recent study by Timp and Zhu, who observed that hydrazine treatment shifts both ionization potential and electron affinity levels compared to NQDs treated with 1,2 ethanedithiol linker.<sup>143</sup> A related study of hydrazine treated PbSe NQD films by Nozik and co-workers found that PbSe NQD films treated with hydrazine in a different solvent

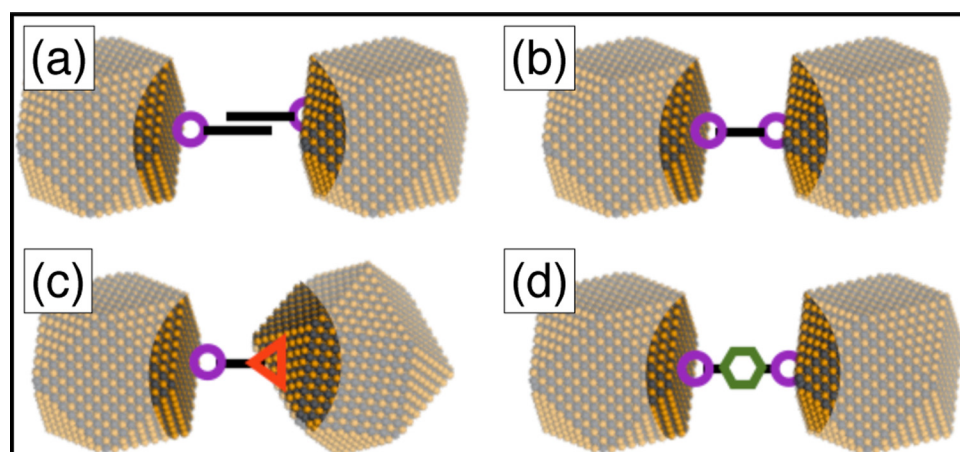


FIG. 14. (Color online) Illustration of various molecular interdot coupling configurations. (a) basic ligand (e.g., ethanethiol), (b) symmetric bidentate linker (e.g., 1,2-ethanedithiol), (c) asymmetric linker (e.g., mercaptopropionic acid), and (d) aromatic linker (e.g., 1,4-benzenedithiol).

exhibited disparate electrical behavior, attributed to subtle differences in adsorbate concentration.<sup>157</sup>

The use of variable length bifunctional linkers allows for systematic tuning of the interdot spacing. Choi *et al.* demonstrated this approach with a series of *n*-phenyl dithiol linkers to illustrate the exponential relationship between exciton dynamics and interdot spacing.<sup>158</sup> As shown in Fig. 15, their study revealed the exponential relationship between interdot spacing and exciton dissociation rate. Importantly, this work also illustrated that coupling-induced tunneling between neighboring NQDs can also split photogenerated excitons in NQD films in absence of electrical or chemical potential gradients. Wolcott *et al.* used variable length alkanedithiol linkers to probe coupling between PbSe NQDs as a function of interdot spacing.<sup>159</sup> The observed redshifts of the NQD exciton absorption peak were attributed predominantly to changes in the polarization of the dielectric environment surrounding

the NQD and to a lesser extent to electronic and transition dipole coupling. In another study using alkanedithiols as a variable length spacer, Law and co-workers demonstrated that carrier mobility decreases exponentially with increasing linker length as expected for hopping transport in granular conductors.<sup>160</sup> They also reported a study of the charge transport characteristics of lead salt NQD films treated with short-chain acids and diacids.<sup>161</sup> This study investigated the impact of several of the linker considerations discussed above and illustrated the complex interplay of surface chemistry, oxidation, carrier mobility and lifetime. The comparison of formic, acetic, and oxalic acid treated NQDs demonstrated the role of linker length and denticity; highest mobilities were observed with formic acid treated PbSe NQD films. The effect of anchor groups was demonstrated in the comparison of carboxylic acid and thiol treated NQD films. Slower oxidation and evolution of carrier mobility were attributed to the more robust binding of carboxylate than thiol groups. Moreover, the study also illustrated the role of electronic coupling and the density of surface traps by comparing the mobility of similarly treated PbSe and PbS NQD films and found that the mobility in the former was tenfold higher.

Short-chain bifunctional linkers such as 1,2-ethanedithiol (EDT), 1,2-ethanediamine (EDA), or 1,4-benzenedithiol (BDT) have emerged as common agents used to couple lead salt quantum dot films. Luther *et al.* reported a comprehensive study of the effect of EDT treatment on structural, optical, and electrical properties of PbSe NQD films.<sup>162</sup> PbSe NQD films coupled with EDA were shown to be beneficial for improved photovoltaic performance,<sup>163</sup> enhanced hot-carrier cooling and ultrafast spectral diffusion.<sup>164</sup> The comparison of EDT and BDT illustrates the effect of the chemical nature of the spacer on the interdot coupling. Although EDT is a slightly shorter than BDT and thus leads to stronger wavefunction overlap, recent studies of both PbS (Ref. 147) and PbSe (Ref. 165) NQD films suggested that BDT treatments result in a lower trap density and improved PV device performance and stability.<sup>166</sup> More recently, a report by Asbury and co-workers compared the photovoltaic performance of PbS NQD films treated with mercaptopropionic acid (MPA) and EDT.<sup>167</sup> MPA treated films exhibited a sevenfold higher mobility-lifetime product than PbS NQD linked with EDT; this difference was attributed to a lower density and energetic distribution of charge traps resulting from the ability of carboxylate and thiol linkers in MPA to passivate a broader distribution of surface states.

The selection of interdot linker also critically influenced the performance of NQD-based LEDs. Importantly, the requirements for successful operation of NQD-LEDs are more constrained than for the NQD-PV. Beyond the challenge of achieving efficient interdot transfer common to both NQD-LED and NQD-PV, the LED must also balance charge injection and efficient radiative recombination within the dot. Since many of these processes are sensitive to the coupling between NQD, this balance can be tuned to by tailoring the inter-QD separation using linker molecules of different lengths. Recent work by Bawendi and Bulovic demonstrated that the design constraints can be relaxed by

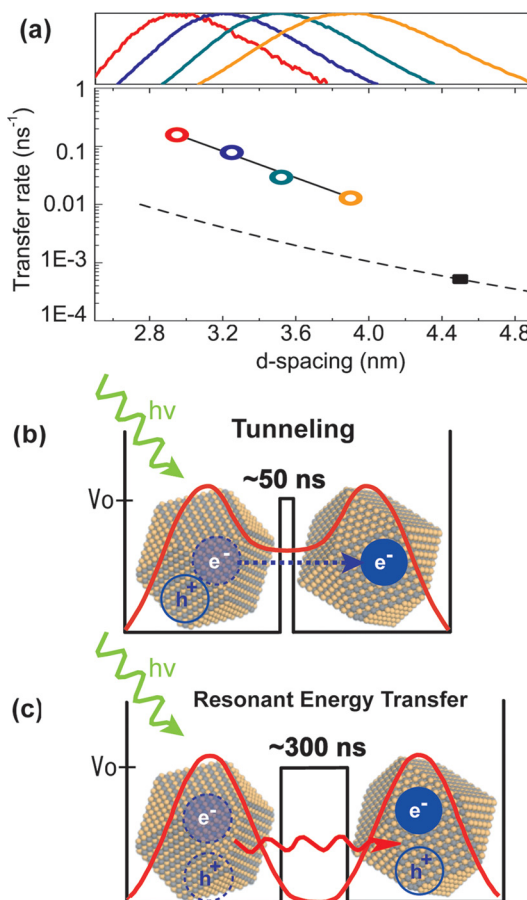


Fig. 15. (Color online) Tunable artificial bond length realized through variable length bifunctional linkers. (a) Charge transfer rates as a function of interdot spacing measured with GISAXS (top panel). Single exponential decay fit (black solid line) indicates that the charge transfer occurs via tunneling of charge through a potential barrier. Resonant energy transfer is shown in the oleic acid passivated NQD (black rectangle) and the calculated energy transfer rates (dotted line) for corresponding interdot spacing using a Förster radius of 5 nm shows an order of magnitude lower rate than the charge transfer rates. This indicates that exciton dissociation via tunneling is the dominant pathway in the regime of short interdot distance and high coupling energy (b) whereas resonant energy transfer is dominant in low inter-NC coupling regime (c). All calculated transfer rates have error bars smaller than the symbols. [From Choi *et al.*, Nano Lett. **10**, 1805 (2010)].

electric field-driven ionization to locally generate carrier pairs needed for electroluminescence.<sup>168</sup>

The linker considerations also apply to the case of electronic coupling between dissimilar nanostructures; for example, from NQD to external electron or hole acceptors. Wise and co-workers recently reported a systematic study of the electronic coupling of PbS NQDs and titania as a function of linker length, anchor group, and the nature of the spacer.<sup>169</sup> It was shown that electron transfer rates decreased systematically with increasing spacer length. The type of anchor group dramatically influenced electron transfer, whereas the nature of the spacer showed little effect. It is important to reiterate that the nature of the linker group also directly influences the discrete energy levels of the NQD itself as was illustrated in the study of PbSe NQDs linked to ZnO using either EDT or hydrazine.<sup>143</sup> The design and development of bifunctional linker molecules optimized for charge transfer in heterojunction PbS NQD/TiO<sub>2</sub> solar cells was demonstrated in a recent paper by Grätzel and co-workers.<sup>170</sup> Taken together, the examples discussed above illustrate how the molecular structure of the linker can be used as a tunable artificial bond to tailor the electronic coupling between NQDs. Although the molecular structure of the organic linker affords broad tunability, organic molecules are generally poor conductors. To address this drawback, new chemical approaches involving inorganic linkers have recently emerged and will be discussed next.

Metal chalcogenide complexes (MCCs) such as zintl ions were introduced by Talapin and co-workers as versatile short inorganic ligands for NQDs.<sup>5,171,172</sup> In contrast to bulky alkyl chain ligands that provide colloidal stability in NQD solutions through steric hindrance, MCCs induce negatively charged NQD surfaces that result in electrostatic repulsion-mediated colloidal stability. Thus, even with the short length of MCCs, a variety of NQDs passivated with MCCs can be dispersed in polar solvents such as water, hydrazine, dimethylsulfoxide, and ethanolamine. Upon deposition on a substrate, MCC-passivated NQDs form structures with short interdot distances and thus strong interdot coupling. In the context of interdot coupling, an attractive aspect of MCCs is that they can be transformed into amorphous or crystalline metal chalcogenide upon mild thermal annealing.<sup>171</sup> Thus, annealing of an MCC passivated NQD superlattice results in a structure where NQDs are embedded in an inorganic semiconductor metal chalcogenide matrix. Since the inorganic semiconductors provide a lower potential barrier between NQDs compared to organic molecules, such structures provide exciting opportunities for achieving strong coupling strength. The case of In<sub>2</sub>Se<sub>4</sub><sup>2-</sup> passivated CdSe NQDs provides an illustrative example of strong electronic coupling and efficient trap passivation as discussed in more detail in Sec. III D. Tangirala *et al.* have demonstrated this approach for a variety of NQDs in inorganic matrices including PbSe/Sb<sub>2</sub>Se<sub>3</sub> and PbSe/GeS<sub>2</sub>.<sup>173</sup> Notably, this approach preserves the superlattice ordering achieved in the initial self-assembly of the colloidal NQD.

Ligand replacement protocols involving inorganic ligands continue to evolve at a rapid pace; several groups

have recently demonstrated the use of metal-free inorganic complexes.<sup>174,175</sup> The most recent development of chemical approaches towards improved interdot coupling involves NQDs passivated with “atomic-ligands.” Sargent and co-workers recently reported a new approach to passivating the NQD surface which involved a two-step process of first displacing the oleic acid ligand with a cadmium-tetradecylphosphonic acid complex to passivate S<sup>2-</sup> anions followed by exposure to cetyltrimethylammonium bromide to introduce bromide ions which passivated the surface cations.<sup>176</sup> PbS NQDs with monovalent halide ion surface passivation exhibited remarkable transport characteristics, which we discuss in Sec. III D.

Solutions to the surface chemistry challenges facing the NQD research community can benefit from the vast knowledge library accumulated in years of microelectronics research on thin films and surface science. Surprisingly, the immense and versatile potential offered by the application of advanced thin film deposition techniques to NQD surfaces has only been explored recently. The applicability of atomic layer deposition (ALD) to form ultrathin conformal passivating layers on NQD thin films is particularly intriguing opportunity. Pourret *et al.* have examined the ALD growth of ZnO on CdSe NQDs drop cast onto quartz substrates, forming films of 50–100 nm in thickness.<sup>177</sup> In this work, pretreatment of the NQD array with NH<sub>4</sub>OH helped initiate ligand removal, and improved the penetration of the ZnO coating. The ability of ALD to functionalize the interstitial volume of the NQD solid has important implications on the performance of NQD devices. In the case of LEDs created from CdSe/ZnS NQDs and passivated with ALD-deposited Al-doped ZnO, Likovich *et al.* recently demonstrated high current densities directed through the NQD as opposed to short circuit through the interstices in films not treated with ALD.<sup>178</sup> Law and co-workers illustrated that ALD processing protects PbSe NQD films from oxidative and photothermal damage<sup>179</sup> and yields NQD films with electron mobilities of 1 cm<sup>2</sup> V<sup>-1</sup> s<sup>-1</sup>.<sup>180</sup>

Physical processing methods towards enhanced interdot coupling in NQD solids must accomplish a delicate balance of coupling proximate dots and while conserving their size-tuned properties. Figure 16(a) illustrates the initial assembly of isolated NQD with insulating surface ligands. Complete deprotection of the NQD surface may lead to coalescence resulting in a polycrystalline bulklike system [Fig. 16(b)]. The “sweet spot” is the idealized *confined-but-connected* structure shown in Fig. 16(c) in which proximate NQD “just touch.” Previous efforts to accomplish this balance have included thermal annealing,<sup>157,181</sup> high-pressure treatments,<sup>182,183</sup> and plasma processing.<sup>184</sup> Thermal annealing NQD thin films in vacuum environment has shown to reduce the interdot spacing and increase the electronic coupling between the NQDs. The reduction in interdot spacing is a direct result of thermally induced removal, curling or interdigitation of surface ligands or evaporation of residual solvents within the NQD superlattice.<sup>185–188</sup> Several studies have utilized the thermal annealing method to tune the interdot coupling and characterized the degree of coupling using scanning tunneling spectroscopy and field effect transistor

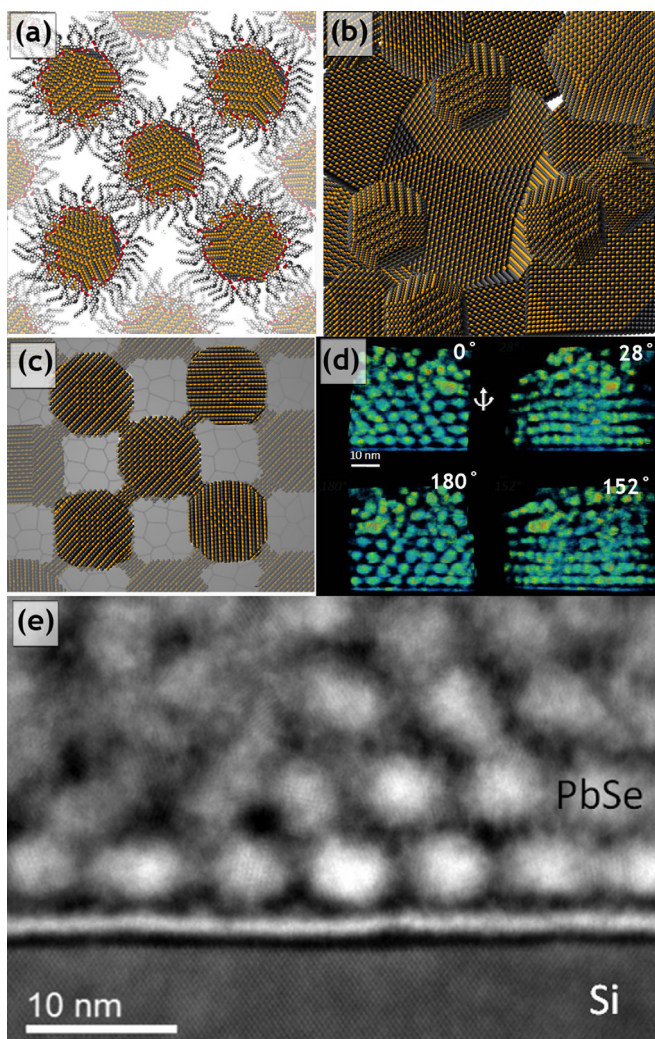


FIG. 16. (Color online) Illustration of confined-but-connected structures. (a) Colloidal NQD coated with organic ligands are strongly confined but isolated from one another. Complete coupling of the NQDs leads to nonfunctional sintered polycrystalline structures (b). The ideal case—a confined-but-connected structure that balances quantum confinement and coupling is illustrated in (c). (d) Tomographic reconstruction of a laser annealed PbSe NQD film and (e) cross-sectional annular dark field scanning transmission electron microscopy image of a PbSe/a-Si nanocomposite film annealed by a laser pulse. [From Baumgardner *et al.*, ACS Nano **9**, 7010 (2011)].

measurements; a significant increase in coupling energy and conductivity was found.<sup>185–193</sup>

A critical drawback of conventional thermal annealing is that the NQDs are prone to sinter under conditions far below the melting point of the corresponding bulk material. *In situ* TEM measurements by van Huis *et al.*<sup>194</sup> showed that PbSe NQDs fuse via oriented attachment at temperatures close to 100 °C, far below the melting point of bulk PbSe (1079 °C). Thermal annealing of self-assembled PbSe NQD superlattices leads to a loss of positional ordering and eventually sintering at temperatures above 168 °C.<sup>186</sup> To avoid coalescence of the NQDs during thermal annealing, nonequilibrium thin film processing techniques have emerged as a promising approach to enhance interdot coupling. Baumgardner *et al.*<sup>195</sup> recently demonstrated pulsed laser annealing as a promising approach to transform self-

assembled PbX NQD superlattices into *confined-but-connected* structures without the mesoscale sintering encountered in thermal annealing [see Figs. 16(d) and 16(e)].

The application of pressure presents an obvious and convenient route to reduce the interdot separation in NQD assemblies. Importantly, the use of external pressure to tune the interdot spacing does not involve chemical changes of the NQD surface which can lead to changes in the NQD electronic structure that obscure the fundamental relationship between interdot spacing and electronic coupling. Early studies of 2D metal nanoparticle superlattices compressed in a Langmuir–Blodgett (LB) trough illustrate systematic changes in the NQD properties as a function of interdot spacing. Heath and co-workers have utilized the LB techniques to precisely and reversibly tune the coupling between Ag nanoparticles with short alkanethiol ligands.<sup>36,196</sup> Combined with optical and electrical characterization, including reflectance, transmission, second harmonic generation, and frequency dependent complex impedance spectroscopy, they demonstrated Mott–Hubbard metal–insulator transition in the Ag nanoparticle monolayer as the internanoparticle surface to surface separation becomes smaller than 1 nm. Yang and co-workers have utilized the LB technique to widely tune the optical response of assemblies of larger (100 ~ 250 nm) Ag nanoparticles.<sup>197,198</sup> In the regime of low nanoparticle packing, they observed Bragg scattering; with interdot spacing smaller than 40 nm, near-field plasmon coupling was observed. In the limit of densely packed nanoparticle films with interdot spacing less than 2 nm, they observed surface plasmons delocalized throughout the entire nanoparticle assembly.

Similar experiments of 3D NQD assemblies within a high-pressure diamond anvil cell are beginning to emerge. Wu *et al.*<sup>183</sup> demonstrated the pressure-driven transformation of gold nanoparticle assemblies into 3D nanostructured architectures with controlled fusion of the particles along the close packed direction of the initial assembly. The transformation of PbS NQD assemblies into 2D single-crystal PbS nanosheets under high pressure inside a diamond anvil cell was recently reported by Wang *et al.* (see Fig. 17).<sup>182</sup> The pressure-induced shape transformation of PbS NQD appears to depend on the dot size and possibly surface chemistry, similar high-pressure experiments by Podsiadlo *et al.*<sup>199</sup> showed that slightly larger PbS NQDs do not fuse and maintain translational order at pressured up to 50 GPa. With new insights into physical processing methods of NQD films, refined control over the structural transformations of the NQD building blocks are likely to emerge. For example, control over the partial fusion of neighboring NQD in ordered superstructures may lead to the creation of NQD solids with programmed crystalline artificial bonds connecting the dots. A theoretical study by Sayle *et al.*<sup>200</sup> mapped out the rich diversity of nanostructures that could be formed if controlled connections between NQDs in periodic assemblies could be achieved.

### C. Self-assembly of superstructures—tuning artificial crystals

NQD research has moved rapidly beyond the synthesis of building blocks with well-defined size, shape, and

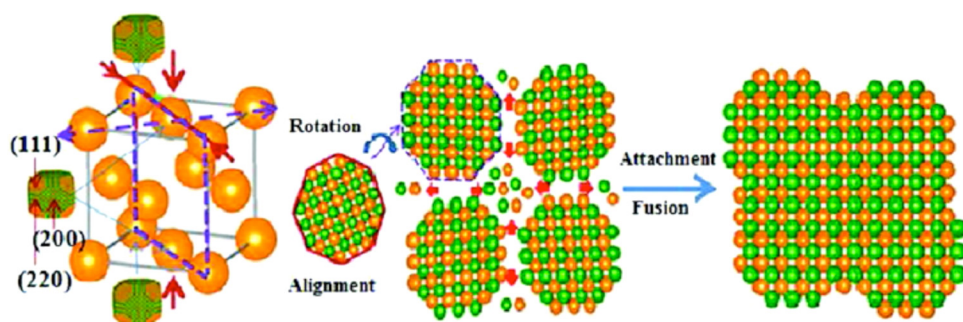


FIG. 17. (Color online) Pressure-driven transformation of NQD assemblies. PbS nanosheets were synthesized by deviatoric stress-driven orientation and attachment of colloidal NQD. [From Wang *et al.*, J. Am. Chem. Soc. **133**, 14484 (2011)].

composition towards the controlled assembly of ordered superstructures. Controlling the self-assembly of NQD solids has important implications on the ability of the constituent NQDs to purposefully interact with each other and their surrounding environment. The challenges associated with creating artificial NQD solids via the self-assembly of colloidal particles into ordered superstructures span multiple length scales. At the nanometer length scale, the interdot coupling is very sensitive to the width and heights of the interdot barriers. As discussed in Sec. II, the interplay of coupling strength and disorder (see Fig. 8) is intimately linked to how closely the NQDs are spaced from one another and how they are oriented relative to one another. At micrometer length scales, the NQD film should be homogenous and crack free. For instance, in optoelectronic applications homogeneous NQD thin films are required to ensure uniform charge transport and light absorption while crack-free films are critical for conformal multilayer processing. At even larger length scales, there is a growing need to translate insights gained from NQD thin film processing in the laboratory to technological processes at commercial scales. This need is most prominently illustrated in the proposed application of NQD in next-generation photovoltaic technologies, where NQD films will need to be processed in large area (many square meters) films, at low cost and high throughput.<sup>201</sup>

The nanoscience community has witnessed impressive advances in the directed assembly of nanomaterials into ordered superstructures with progressively improving control over superlattice spacing, symmetry, and grain size. This progress has been enabled by the combination of the availability of high quality nanomaterial building blocks and enhanced fundamental understanding physical and chemical aspects underlying the directed self-assembly. The field has evolved from the assembly of monodisperse metal<sup>202</sup> or semiconductor particles<sup>39</sup> into highly ordered superlattices towards the directed assembly of superstructures that mirror the diversity of crystal symmetries encountered in atomic crystals. Recent work by Mirkin and co-workers provides a prominent example demonstrating the structural diversity of nanoparticle superlattices achievable with DNA as a programmable linker.<sup>203</sup> The directed self-assembly of binary<sup>204</sup> and ternary<sup>205</sup> nanoparticle superlattices, assemblies of complex shaped nanostructures<sup>206,207</sup> and self-assembly of supraparticles from polydisperse nanoparticles<sup>208</sup> provide further

examples of the rapid progress in the field. A comprehensive review of the advances in nanomaterial self-assembly is not practical here; several reviews are available in the literature<sup>5,209</sup> and a recent book by Kotov provides an excellent resource.<sup>210</sup> Below, we review fundamental and practical aspects of creating NQD solids via self-assembly of colloidal semiconductor nanoparticles. We demonstrate how the structure of the NQD solids can be adjusted as the third tunable parameter of the properties of artificial solids.

To understand and control the self-assembly of NQD superstructures a variety of interparticle forces including van der Waals, electrostatic, magnetic, molecular, and entropic effects need to be considered. A recent review by Grzybowski and co-workers provides a comprehensive summary of the relative contribution of these forces in directing the self-assembly as a function of the magnitude and length scale of the interaction.<sup>211</sup>

To a first approximation, the interaction between colloidal nanoparticles can be described by a hard sphere interaction potential. Analogous to the Lennard-Jones potential commonly used to describe the interaction of spherical atoms, similar models with characteristic interaction length scale and energy have been applied to model isotropic pair interaction potentials of colloidal and nanoparticle systems. The van der Waals attractions are balanced by excluded volume interactions of ligands bound to the particle surface of hard spheres. Compared to metal nanoparticles, the van der Waals interactions between semiconductor nanocrystals cores are relatively weak and the interactions are in most cases screened by the steric repulsion of the surface bound ligands.<sup>212</sup> The hard sphere model predicts the equilibrium structure of size-monodisperse spheres as a close-packed face-centered cubic (fcc) superlattice. Evers *et al.* have also shown that self-assembled binary superlattices of weakly interacting semiconductor NQDs form in accordance with the hard sphere model.<sup>212</sup> Although many nanoparticle systems self-assemble into superlattices with fcc symmetry, there are also numerous examples of superlattices with nonclose packed symmetries as discussed below.

A closer look at the colloidal NQD shown in the molecular dynamics model snapshot of a particle and its surrounding ligand shell [see Fig. 3(b)] suggest that the particle and the surrounding ligand shell may not be accurately described as a hard sphere. Given the complex interactions of the

nanoparticle, the surface bound ligand and the surrounding solvent molecules, deviations from the hard sphere model are not very surprising. Instead, the molecular dynamics of the ligand shell are more appropriately captured in a soft sphere model in which the softness of the ligand shell can be parameterized by the ratio ( $\chi$ ) of the ligand length ( $l$ ) to the particle radius ( $r$ ) (i.e.,  $\chi = l/r$ ).<sup>213,214</sup> Colloids and relatively large diameter NQD up to  $\chi \sim 0.7$  interact as hard spheres and form close-packed assemblies with fcc symmetry. In contrast, softer NQD, beyond  $\chi > 0.7$ , favor more open structures in which the flexible ligands occupy interstitial space in the body-centered cubic (bcc) superlattice.<sup>213,214</sup>

The actual 3D shape of the nanoparticle presents an obvious perturbation to the soft sphere model. The diversity of available nanoparticle shapes has profoundly expanded the range of possible self-assembled superlattice symmetries.<sup>206,215</sup> Two recent studies by Heinze *et al.*<sup>216</sup> and Damasceno *et al.*<sup>217</sup> illustrated how nanoparticles with programmed polyhedral shapes can be directed to self-assemble into densest packing superstructures. Even if the colloidal

NQDs appear quasispherical in TEM images, various superlattice polymorphs may be observed. A recent study of the self-assembly of oleic acid passivated lead salt NQDs, Hanrath and co-workers illustrated that details of the NQD shape and molecular interactions between the ligands and solvents need to be considered to understand how identical NQDs can be directed to self-assemble into superlattice polymorphs with fcc, bcc, and body-centered tetragonal (bct) symmetry.<sup>218</sup> Figure 18 shows grazing incidence small angle x-ray scattering (GISAXS) patterns of PbS NQD superlattice polymorphs. By analogy to atomic crystals, the lattice symmetry transformation can be understood as a Bain deformation.<sup>219</sup> In a related study, the same group demonstrated how the self-assembly can be directed towards predefined superlattice symmetries by exploiting the anisotropic ligand coverage on specific NQD facets.<sup>220</sup> Specifically, PbS NQDs with dense ligand coverage were found to assemble into fcc superlattices whereas NQDs with sparse ligand coverage assemble into bcc superlattices which also exhibit orientational ordering of NQDs in their lattice sites as confirmed by

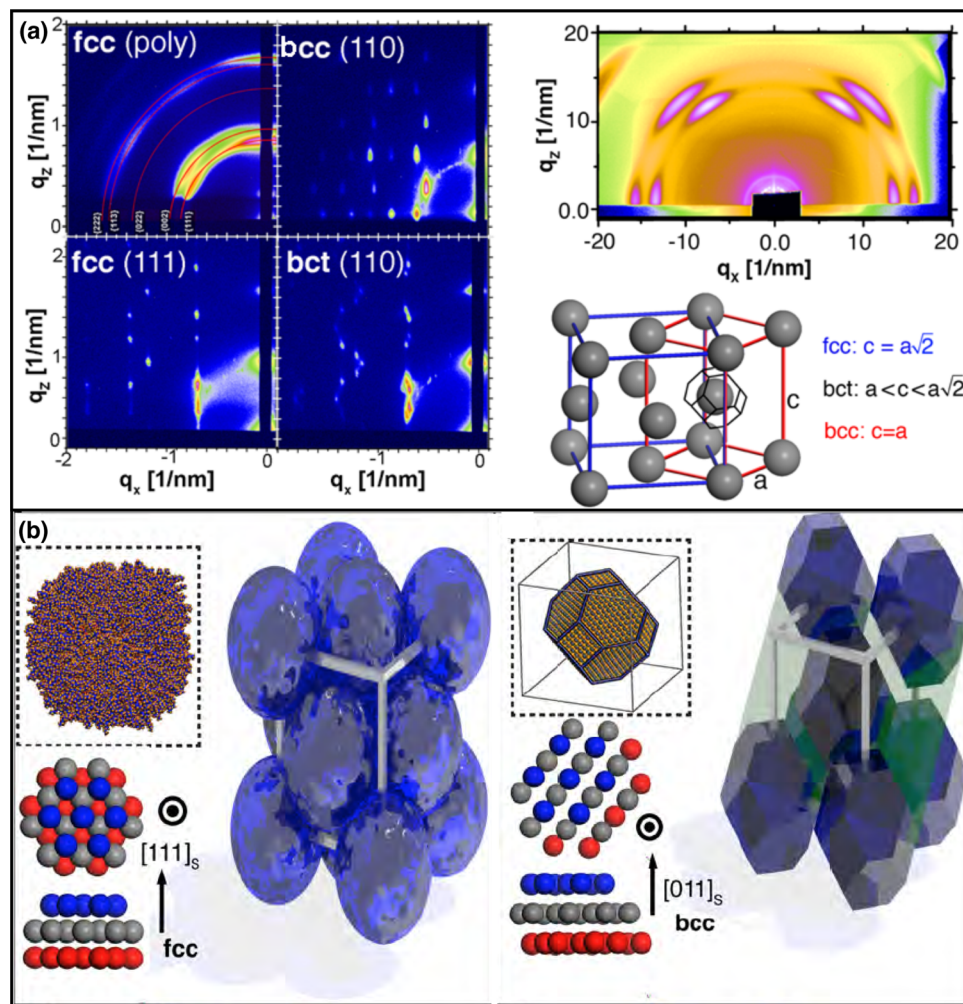


FIG. 18. (Color online) Controlling the structure of self-assembled NQD superlattices. (a) GISAXS patterns of PbX NQD assembled into fcc, bcc, and bct superlattices. The model shows how the crystal symmetries are related through the Bain deformation. The wide-angle scattering (top right) shows the orientational ordering of PbS NQD in the lattice sites of the bcc superlattice. (b) Illustration of the relationship between particle shape and superlattice symmetry. Particles with an isotropic interaction potential behave as spheres and assemble into fcc superlattice; cuboctahedra particles exhibit anisotropic interactions and assemble into bcc superlattice with orientational ordering of the particles in their lattice sites. [From Bian *et al.*, ACS Nano 5, 2815 (2011).]

the wide-angle scattering pattern in top left of Fig. 18(a). A similar recent study by Zhang *et al.* correlated the evolution of PbS NQD shape from cubic to quasispherical to a continuous transformation of the superlattice symmetry from simple cubic to rhombohedral phases.<sup>221</sup>

The combined control over translational and orientational ordering of NQD is an advantageous experimental degree of freedom to tailor the interdot coupling within the assembly. However, to date, theoretical predictions and comparison to experiment are scant. Density functional theory calculations of metal nanoparticle dimers predict that the relative orientation between the particles is a critical determinant of the coupling strength.<sup>222</sup> Effective mass quantum mechanical calculations of two-dimensional QD assemblies indicate that orientational alignment of neighboring QDs can significantly enhance the quantum coupling energy.<sup>187</sup>

It is important to note that the anisotropy introduced by the interactions of NQD facets on proximate particles introduced a directionality of the interaction potential. In combination experimental control over the translational ordering and orientational ordering offers a valuable degree of freedom to tune the degree of (dis)order in the NQD solid and sets a promising stage for investigations of structure-property relationships in context of the electronic structure phase diagram shown in Fig. 8.

The polydispersity of both particle size and shape is an important experimental parameter in the preparation of ordered superlattices.<sup>223</sup> In the case of spherical or quasi-spherical particles, the void space in the assembled structure provides some tolerance for polydispersity so that ordered superlattices can still be formed with particles up to about 10% relative size distribution. The tolerance for polydispersity in the self-assembly of space-filling polyhedra is much less although theoretical limits remain to be resolved.

Electrostatic interactions present significant perturbation to the basic hard sphere model. Repulsive and attractive Coulombic interactions between particles with like and dislike charges have been studied in colloidal and nanoparticle assemblies.<sup>210</sup> The interaction potential of charged colloids dispersed in an electrolyte is captured by the Derjaguin and Landau, Verwey, and Overbeek (DLVO) pair potential interaction.<sup>210,211</sup> Electrostatic effects can also give rise to directional interactions, e.g., through dipole-dipole interactions. In the specific case of PbX NQDs, dipoles are believed to arise from an uneven distribution of Pb- and Se-terminated {111}NC facets of individual NQDs<sup>121</sup> with cuboctahedra shapes or charged surface states.<sup>224</sup> Dipole pair interactions, whose strength was recently estimated to be in the range of 8–10 k<sub>B</sub>T,<sup>225</sup> have been attributed as the driving force in the formation of highly anisotropic nanostructures, via oriented attachment,<sup>122,226</sup> and the assembly of NQD films with nonclose-packed, simple hexagonal symmetry.<sup>227</sup> The origin of the dipole in PbSe NQDs and the detailed atomic structure of the NQD facets remain a topic of ongoing investigation. Analytical studies of lead salt NQDs have indicated that the composition of dots varies significantly depending on synthesis parameters and is, in most cases, characterized by an excess of lead.<sup>162,228</sup> Recent theoretical and experimental

work by Fang *et al.* suggested that the {111}NC facets are composed of ribbons of alternating polarity that are stabilized in the presence of surface bound ligands and in their absence transform to ribbonlike Pb or Se nanodomains.<sup>229</sup> New insights into the physical and chemical nature of the NQD facets continue to emerge from ongoing studies. Although the complex relationship between the atomic structure of the NQD and its optoelectronic properties is recognized, many important fundamental questions remain; the surface chemistry challenges are discussed in more detail in Sec. IV.

We now turn to practical considerations of forming ordered NQD superlattices. The self-assembly of NQDs into ordered superlattices resides naturally at the intersection of molecular crystal growth and the assembly of micrometer sized colloids. Whereas the crystallization of atomic crystals is generally a rapid process, colloidal crystals generally take days to months to form.<sup>230</sup> At intermediate length- and time-scales NQD superlattices typically form within minutes; this is an experimentally advantageous time scale and enables *in situ* studies<sup>218,231–233</sup> as well as control over the superlattice symmetry by adjusting the crystallization dynamics.<sup>234,235</sup> To build on the analogies between classical and artificial crystals introduced earlier, it is helpful to consider parallels between crystallization of atomic solids and the self-assembly of NQD superlattices. In marked contrast to the rapid nucleation and growth required for colloidal NQD synthesis discussed above, the formation of large grain atomic crystals and NQD superlattices is performed under conditions favoring minimal nucleation and slow growth. Single crystals; for example, the growth of single crystal Si boules via the Czochralski process, are obtained from a single nucleation source in a system maintained at low supersaturation. Similar considerations guide the growth of highly ordered large grain NQD superlattices.

Interface effects are known to play a central role in the nucleation and growth processes of atomic and colloidal crystals alike. At intermediate length scales, NQD superlattice nucleation can occur heterogeneously at a two-phase interface, e.g., substrate/solution,<sup>236</sup> gas/solution,<sup>196,237,238</sup> or homogeneously within the colloidal NQD suspension.<sup>239</sup> *In situ* characterization techniques continue to provide important new insights to the superlattice growth processes. For example, Jiang *et al.* recently demonstrated the formation of crystalline 2D superlattice domains at the gas/suspension interface during droplet evaporation.<sup>233</sup>

NQD superlattices are formed from colloidal suspensions of particles by either gradually evaporating the solvent or by destabilizing the colloidal suspension by adding an antisolvent, or precipitant to slowly diffuse into the suspension. Evaporation-driven methods have been the more common route to create monolayer and thin film NQD solids on planar or patterned substrates. Recently, work by Talapin and co-workers illustrated how diffusion limited growth, inspired by protein crystallization techniques,<sup>240</sup> yields high quality, large grain, 3D faceted NQD solids.<sup>241,242</sup> A comprehensive review of wet coating techniques to form nanoparticle superlattices was recently published by Maenosono *et al.*,<sup>243</sup> here we

discuss specific examples of evaporation-driven approaches that have been demonstrated for semiconductor NQD films.

The most basic approach to forming NQD superlattices is by drop-casting the colloidal suspension onto the target substrate and allowing the solvent to evaporate.<sup>202,244,245</sup> The evaporation rate of the solvent can be tuned by either adjusting the volatility of the solvent<sup>244</sup> or by carrying out the evaporation in a slightly subsaturated vapor environment.<sup>234</sup> In some cases, the solvent evaporation is accomplished by evaporating the solvent in an evacuated chamber and allowing the superlattice to grow on a tilted substrate.<sup>227,246</sup> Interactions between the colloidal particles and the substrates can be exploited to template the growth of the NQD film. For example, functionalization of planar substrates with self-assembled monolayers have been applied to pattern the growth of metal and semiconductor NQD thin films.<sup>247–250</sup>

Beyond the drop-casting onto flat planar substrates, there has been increasing interest in the deposition of NQD assemblies and thin films onto patterned 3D electrodes;<sup>251,252</sup> in these cases the spatial ordering of the NQD is perturbed by the geometry of the 3D substrate. Given the continued advances in self-assembly and formation of ordered patterns, significant progress can be expected in this direction.

Despite the simplicity, the drop-casting approach has several drawbacks; most prominently the NQD thin film tend to exhibit micrometer sized fractal pattern reminiscent of cracks found in dried mud or paint. Cracking during the drying of thin films is a well-known phenomenon reoccurring at multiple length scales.<sup>253</sup> The cracks arise from the concurrent volume reduction and adhesion to the underlying substrate which creates lateral stresses within the evaporating thin film that are ultimately relaxed through the formation of cracks. In the formation of NQD thin films for device applications, the cracking effects are exacerbated by ligand exchange treatments and pose a significant challenge in the processing of prototype test structures.<sup>156,157,162,166,254,255</sup>

Dip-coating provides a convenient route to process crack-free NQD films. Importantly, sequential, often automated, dip-coating techniques are readily integrated with solution based ligand exchange and surface chemistry treatments.<sup>162,256</sup> This approach has been successfully applied in a layer-by-layer approach to create crack-free NQD films with carefully controlled thickness; however, the ordering of NQD films is generally lost during the solution-based ligand exchange treatment.<sup>234</sup> Talgorn *et al.* recently exploited dip-coating to create alternating layers of CdSe and CdTe NQD films with varying thickness as a test structure for the study of exciton dissociation dynamics at the CdSe/CdTe interface.<sup>257</sup> Drag-coating<sup>258</sup> and doctor blading<sup>259</sup> present two commonly used derivatives of the “evaporation-driven” approach towards NQD superlattice growth; in both cases, the velocity of the casting blade provides an additional experimental parameter to fine-tune the superlattice growth conditions. Inkjet-printing<sup>260,261</sup> and spray coating<sup>262,263</sup> have significant potential for the high-speed and large-area processing of NQD thin films; however, the solvent evaporation rates encountered in these techniques is generally too fast to allow the nanoparticles to order. Monolayer and

controlled multilayer NQD assemblies have also been formed by controlling the self-assembly at the liquid-air interface. For example, Langmuir–Blodgett,<sup>264</sup> Langmuir–Schaefer,<sup>265</sup> and other modifications of the liquid-air interfacial assembly approach<sup>266</sup> have been demonstrated to yield highly ordered NQD assemblies. These quasi-2D assemblies provide advantageous experimental systems for the study of extended electronic states as discussed in the next section.

Spin-coating provides another convenient route to form NQD thin films. While spin-coating is often the method of choice for the formation of organic thin films, the spin-casting of ordered multilayer NQD films is complicated by the fact that the rapid recession of the vapor-liquid interface often does not permit sufficient time for the NQD to rearrange into ordered structures. This complication can be overcome in thin NQD assemblies and monolayers by tuning the evaporation dynamics; e.g., Coe-Sullivan *et al.* demonstrated that large area ( $> \text{cm}^2$ ) NQD monolayers can be formed by spin-casting a mixed solution of aromatic organic materials and aliphatically capped NQD.<sup>238</sup>

We conclude this section with a brief discussion of the techniques applied to characterize the ordering in NQD superlattices. Scanning electron microscopy (SEM) and TEM are generally the first choice in the morphological characterization of nanomaterials and their assemblies. For example, SEM characterization has been used in combination with analysis of either their Fourier transform or the autocorrelation function.<sup>267</sup> TEM characterization offers several advantages including direct visualization of the assembly and the projected shape of the constituent particles as well as electron scattering to probe the orientational ordering of the NC in the assembly.<sup>268</sup> Recent advances in electron tomography have introduced the possibility to characterize structural defects in the NQD solids.<sup>190,205,269</sup> However, TEM analysis is generally limited to a small fraction of the sample assembled on a TEM support grid.

X-ray scattering techniques provide arguably the most accurate and detailed characterization of superlattice structure, although structure must be inferred from  $k$ -space scattering images instead of the direct images provided by electron microscopy. The scattering patterns provide highly detailed structural information including not only the symmetry and the spacing of the superlattice but also vertical or horizontal variations in the lattice constant. The combination of wide-angle and small-angle x-ray scattering is particularly beneficial since it provides information about the orientational and translational ordering of NQDs in the assembly, respectively. Scherrer peak width analysis can be used to determine both the vertical and horizontal superlattice grain size.<sup>218</sup> Moreover, advances in *in situ* x-ray scattering techniques have allowed researchers to monitor the reversible self-assembly in real time and under controlled assembly conditions.<sup>30–32,218</sup>

## D. Electronic structure and charge transport in NQD solids

Experimental analysis and characterization of the electronic structure of NQD solids is based largely on charge

transport measurements, optical spectroscopy, or tunneling spectroscopy; we review several examples below. Charge transport measurements, generally at variable temperatures, provide crucial experimental insights into the interplay of coupling, disorder, and charging energy that define the electronic phase diagram discussed in Sec. II (Fig. 8). Guyot-Sionnest recently summarized the requirements for efficient charge transport through NQD solids in four golden rules, which are (i) there must be stable and partial occupation of a lowest NQD state, (ii) the NQD must be stable under reduction or oxidation although there cannot be a large dynamic trap density, (iii) the charges must be able to move, so the interdot barriers cannot be too high or too wide, and (iv) there will inevitably be disorder.<sup>270</sup>

If interdot coupling is weak, charge transport through the NQD film occurs via activated hopping from dot to dot. Fundamentally, the energetics and kinetics of the interdot hopping are derived from Marcus theory of electron transfer. Hopping between nearest neighbors is the most basic case; however, if the variation in barrier width and site energy dispersion are large, hopping to a dot that is not the nearest neighbor may be energetically more favorable even though the hopping distance is larger. A detailed discussion of the relevant hopping mechanisms can be found in the review of granular electronic systems by Beloborodov *et al.*<sup>271</sup> The different hopping transport mechanisms can, in principle, be experimentally distinguished by measuring charge transport at variable temperatures. The temperature-dependent conductance can generally be described by  $\ln\sigma_{(T)} \sim (1/T)^v$ . In the case of simple (nearest-neighbor) hopping transport, thermally activated (Arrhenius) behavior is observed and  $v=1$ ; this trend was reported in lead salt NQD films by the groups of Kastner<sup>188</sup> and Murray.<sup>272</sup> In the variable-range hopping model introduced by Mott,<sup>63</sup>  $v=1/4$  for transport through a 3D system. Accounting for Coulombic interactions between the electrons, as was done by Efros and Shklovskii,<sup>273</sup> modifies the temperature dependence to  $v=1/2$ . Since Coulombic interactions are less significant at high temperatures, a transition from  $v=1/2$  to  $v=1/4$  behavior is expected with increasing temperature; this trend was reported by Guyot-Sionnest and co-workers and is shown in Fig. 19(a).<sup>274</sup> Caution is warranted, however, in the interpretation of variable-temperature conductance by fitting to a basic model. The intricacies of charge transport through complex NQD solids and potential pitfalls of oversimplified models were illustrated in the recent work by Houtepen *et al.*,<sup>275</sup> their study of charge transport through ZnO NQD films were described by  $v$ , which was explained as an adaptation of the Efros-Shklovskii variable range hopping model. The hopping transport examples illustrate that charge transport in NQD solids has more in common with molecular systems and granular solids than bulk semiconductors.

Trapping of mobile carriers in poorly passivated surface states is an important consideration in the charge transport through NQD films. An early study by Ginger and Greenham explained charge injection and transport in CdSe NQD films based on a space-charge limited transport model with trapping of mobile carriers in deep traps.<sup>276</sup> Current decay mea-

urements revealed electron mobilities on the order of  $10^{-6} \text{ cm}^2 \text{ V}^{-1} \text{ s}^{-1}$ , which corresponds to a trap density of  $2(10^{16}) \text{ cm}^{-3}$ , or 1 per 100 NQDs in the film. More recently, Napal and Klimov investigated the role of traps states via optical field effect transport measurements;<sup>277</sup> their study showed that charge transport in the dark occurs through coupled midgap states whereas under illumination, charge transport through the NQD film is dominated by a more conductive network of quantized states. The density and energetic depth of the traps poses significant limitations to the performance of NQD films in PV or photodetector applications. Remarkable enhancements in device performance can be directly attributed to improved understanding and control of surface

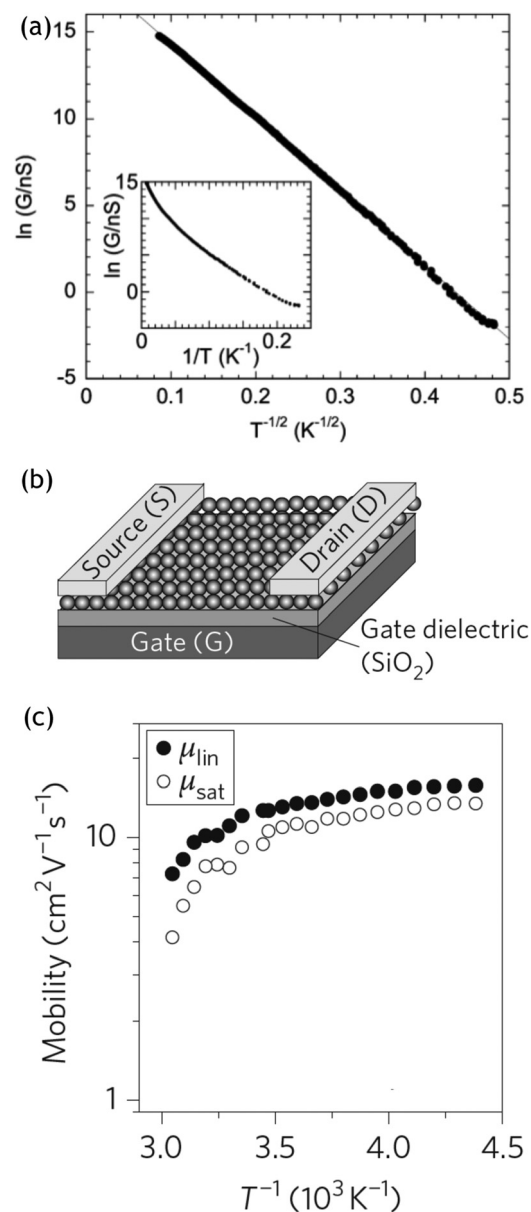


FIG. 19. Charge transport through NQD thin films. (a) Low bias (20 mV) conductance of PbSe NQD films shows temperature-dependent signatures consistent with variable range hopping [from Wehrenberg *et al.*, J. Phys. Chem. B **109**, 20192 (2005)]. (b) Schematic of a field-effect transistor test structure with NQD film as the channel device, (c) temperature dependence of field-effect mobility for an *n*-channel device assembled from  $In_2Se_3$ -capped 3.9 nm CdSe NQD.

chemistry treatments to limit the defect trap density.<sup>176,278,279</sup> In the most recent example, the Sargent group demonstrated higher mobility and shorter trap-to-band transition time of bromide-passivated PbS NQDs compared to the conventional EDT-coupled NQD films. This approach afforded both enhanced electronic transport and passivation of surface states, which enabled the fabrication of NQD solar cells with up to 6% conversion efficiency. The significant role of NQD trap density on the future improvements of NQD-based PVs was summarized in a recent review by Kramer and Sargent.<sup>280</sup>

Confirmation of the theoretically predicted Blochlike band structure in NQD solids is discussed in Sec. II, has been complicated by the experimental challenges associated with achieving sufficient interdot coupling, low density of electronic traps and low energetic disorder. In contrast to thermally activated hopping, bandlike charge transport through delocalized states of the NQD solid is characterized by decreasing mobility and conductivity with increasing temperature; two recent studies of charge transport in CdSe (Ref. 281) and PbSe (Ref. 282) NQD films have reported such behavior. Talapin and co-workers investigated CdSe and CdSe/dS NQD films coupled with metal chalcogenide complexes and demonstrated high electron mobility (up to  $16 \text{ cm}^2 \text{ V}^{-1} \text{ s}^{-1}$ ) which decreased with increasing temperature [see Fig. 19(c)].<sup>281</sup> The Siebbeles group probed photoconductivity and quantum yield of strongly coupled PbSe NQD films and pointed to the temperature-invariant photoconductivity as an indication of bandlike charge transport.<sup>282</sup> These two examples show how advances controlling the interdot coupling have enabled progress towards charge transport properties approaching those of bulk crystalline semiconductors.

Beyond the improved charge transport characteristics of coupled NQD films, there have also been several intriguing experimental demonstrations of collective properties of NQD solids arising from quantum mechanical interactions. Murray and co-workers<sup>283</sup> demonstrated a 100-fold enhancement in conductivity of 1:1 binary PbTe/Ag<sub>2</sub>Te NQD superlattice compared to the conductance of the single-component NQD films. This synergistic effect elegantly illustrated the role of Ag<sub>2</sub>Te as a *p*-type dopant in PbTe NQD solids.<sup>284</sup> The same group has recently reported temperature-dependent thermopower measurements on the same experimental system to illustrate the effect of artificial atom doping on the electronic structure of the NQD solids.<sup>272</sup> Their work revealed similarities and differences compared to doping in traditional semiconductors and illustrated opportunities for tuning the electronic structure of NQD solids. Experimental control over interdot coupling in NQD solids also has important implications on the study and creation of magnetic metamaterials; this effect was elegantly illustrated in the recent report of collective dipolar interactions in binary superlattices of Fe<sub>3</sub>O<sub>4</sub> nanocrystals by Chen *et al.*<sup>285</sup>

Comparison of NQDs in the solid (i.e., thin films) with isolated NQD in the colloidal suspension *can* provide first indications of interdot coupling; however, the optical spectra of NQD films need to be interpreted with caution to properly

distinguish quantum-coupling signatures from other effects such as the change in the dielectric of the NQD film and modifications to the NQD surface accompanying the physical or chemical coupling treatment. Direct observation of quantum coupling of the electronic states has been proven in the splitting of energy states probed by PL of MBE-grown GaAs NQDs grown in a GaAlAs matrix.<sup>61</sup> In the case of colloidal NQD thin films, several groups have interpreted redshifted optical spectra as an indication of increased interdot coupling in the condensed state. Döllefeld *et al.* have pointed out that there are several experimental pitfalls that require careful consideration to distinguish electronic from dipole-dipole interactions.<sup>286</sup>

Scanning tunneling spectroscopy (STS) has established itself as an advantageous characterization for investigating the detailed electronic structure of NQDs.<sup>60</sup> The Vanmaekelbergh group has applied STS to probe variable orbital coupling in 2D NQD solids; analysis of the tunneling spectra allowed them to distinguish between coupling of only the conduction electrons from full delocalization of both electron and holes.<sup>187</sup> The same group later reported another elegant experiment involving coupled NQD molecules in the form of PbSe NQD dimers, trimers, etc., surrounded by wide gap CdSe NQD as an inert matrix; this study provided quantitative insights into the electronic local density of states and interdot coupling and the extent of delocalization in NQD.<sup>287</sup>

#### IV. SUMMARY AND CONCLUSION

We hope that this review captured some of the remarkable advances in fundamental research and technological development of semiconductor NQDs. In the approximate two decades since the seminal reports on colloidal NQD synthesis and their fundamental structure-property relationships, the field has grown immensely and evolved from the creation of isolated NQDs with programmable optoelectronic properties to their directed self-assembly into functional superstructures. The concept of NQD assemblies as artificial solids has matured from a predominantly theoretical model to a guiding principle for the study and engineering of NQD solids with properties by design. Improved understanding and control over the NQD surface properties have been vital in this development; in fact, it is difficult to overstate the critical role of the interfacial properties from the initial growth and stabilization of NQDs to the controlled coupling and self-assembly. Despite this immense progress, critical fundamental knowledge gaps remain. From a technological perspective, the development of NQD-based devices risks stalling in its rapid progress if current challenges concerning interdot coupling and device integration are not resolved. In the outlook below, we provide three examples of unresolved challenges in the road ahead: (i) the detailed physicochemical nature of the NQD surface, (ii) the inherent inhomogeneity of the NQD ensemble, (iii) the *true* electronic structure of NQD solid, and (iv) the connection between NQD model systems in the laboratory and commercially deployable NQD technologies.

The detailed physical and chemical nature of the NQD surface remains one of the biggest unknowns. Much work

remains to resolve open questions about the NQD interface including: “Where and how are ligands bound to the NQD surface?” “What is the reconstruction and faceting of the NQD surface and how do surface-bound species influence electronic structure of the NQD and the coupling between them in a solid?” Advances in characterization tools, in particular *in situ* approaches and techniques adopted from the surface science community, will continue to play an important part in the solution to these questions. Our summary of methods to tailor the interdot coupling illustrated how the field evolved from early mass action ligand exchange approaches (i.e., exposing the NQD to excess of the new ligand to drive the exchange) to the application of more advanced surface science techniques, such as ALD, to balance surface passivation and interdot coupling.

The inherently inhomogeneous nature of colloidal NQD ensembles presents an important limitation on their analogy as artificial atoms. In a recent editorial, Talapin and Yin pointed out interesting analogies between the development of polymer chemistry and NQD chemistry.<sup>288</sup> Instead of a fully deterministic system, both fields are faces with ensemble distributions, either polymer chain length or particle size. The future evolution of synthetic NQD science will likely benefit from lessons learned in the preparation and characterization of polymer ensembles. For the NQD research community, the challenge ahead is thus to develop robust synthetic and characterization methodologies to limit and quantify the NQD polydispersity. The NQD diameter distribution presents a good example. Although carefully controlled colloidal NQD synthesis now enable the creation of ensemble diameter distributions with standard deviation as low as 5%, it is important to keep in mind that for a typical NQD diameter ( $\sim 10\text{ nm}$ ) this distribution corresponds to approximately  $\pm 1$  atomic lattice constant. Further refinements in the homogeneity of colloidal NQDs require post-synthesis processing. These techniques have evolved from size-selective precipitation,<sup>289</sup> to chromatographic techniques,<sup>290</sup> and most recently to ultracentrifugation.<sup>291</sup> Access to NQD samples with a narrower diameter distribution will be advantageous in systematic fundamental studies of disorder on the electronic structure of the NQD solids. The particle diameter distribution also has important implications on the development of NQD-based technologies. For example, in LEDs, the polydispersity broadens the emission,<sup>292</sup> in solar cells, the distribution of NQD diameters defines the spectrum of absorbed light, but has less impact on PV performance.<sup>293</sup> Aside from the distribution of NQD core diameters, little is currently known about the ensemble distribution of NQD interface properties such as ligand density or surface reconstruction. Given the sensitive relationship between the NQD’s electronic structure and the nature of its interface, further refinements towards a well-characterized and well-defined surface state are required.

Much of the recent push towards NQD-enabled optoelectronic applications is driven by their potential application in energy technologies. Impressive advances have been achieved with NQD-based PVs, which have rapidly evolved from proof of principle devices to advanced PV structures with conver-

sion efficiencies approaching 6%. NQD-PV follow in the footsteps of organic PVs, albeit with a steeper slope of the efficiency learning curve.<sup>294</sup> This progress is in large part due to advanced understanding of the complex charge transfer processes in the inherently heterogeneous films. Notwithstanding the rapid progress, significant knowledge gaps with regards to the electronic structure and charge transport in NQD thin films remain. Phenomenological models adopted from transport in bulk semiconductors are quickly approaching their limitations since they do not capture the intricate physics of charge transport in a disordered ensemble of NQDs. For example, field-effect transport characteristics of NQD films are commonly described based on the majority carrier as *n*-type, *p*-type, or ambipolar. The NQD in the ensemble, however, are not homogeneously doped, in fact, doping of colloidal NQD remains an unresolved challenge which has been attributed to the “self-purification” effect.<sup>295,296</sup> A typical NQD film contains on the order of  $10^{18}\text{ dots}/\text{cm}^3$  and reported carrier concentrations range from approximately one carrier per dot<sup>161</sup> to one carrier per 500 dots.<sup>16</sup> Instead of being modulated by foreign dopants, the carrier concentration in the NQD films is more closely related to the density and energetic spectrum of electrically active surface states; better theoretical understanding and experimental control over interfacial properties have been essential in the microelectronic revolution and advances in related NQD interface challenges are required to successfully translate the promise of NQDs into a technological reality.

Band bending and depletion width provide additional examples of the limitations of applying bulk semiconductor concepts to describe transport characteristics of NQD films. Although these models have successfully been applied as a guide in the performance enhancements of NQD devices, it must be borne in mind that they do not capture the “true” electronic structure of the junction, which is much more complex due to the presence of myriad nanostructured interfaces. To date, the NQD films used in such device studies are characterized by significant electronic disorder, so that significant delocalization and band formation are not expected. To sustain the rapid pace of progress in NQD-based energy technologies, detailed *ab initio* models of charge transport within and across NQD films are required. Given the tremendous research effort currently directed towards a better understanding of the electronic structure of NQD solids, improved models that account for the true electronic nature of the NQD solid are likely to emerge in the near future.

Finally, the development of NQD-based commercial products must also take underlying environmental and economic aspects into consideration. CdX and PbX NQDs at the focus of this review provide an ideal model system for a fundamental study of artificial solids; however, from a technological perspective, the deployment of NQD-based technologies, in particular, thin film PVs or LEDs containing Pb or Cd, is confronted with several environmental questions arising from the heavy metal toxicity. There are two avenues to address this recognized challenge. The first is that the encapsulation of colloidal NQD in an inorganic matrix (similar to those

discussed in Sec. III B) can substantially reduce or even eliminate risks associated with leaching of the heavy metal out of the device. Arguably, if the NQDs are appropriately processed to protect the core from surface reactions (e.g., oxidation or moisture), then the surrounding environment will *vice versa* be protected from the heavy metal chalcogenide inside the NQD. The second approach is to translate insights gained from the study of PbX and CdX model systems to the development of alternative, environmentally benign, semiconductor NQD materials. Aside from toxicity, recent reviews of potential PV materials have also factored abundance, cost, and performance into consideration.<sup>297,298</sup>

## ACKNOWLEDGMENTS

The author would like to thank the following individuals for their contributions concerning the work reviewed here: Joshua J. Choi, James R. Engstrom, and Frank W. Wise. The author would also like to acknowledge funding of this research from the National Science Foundation (NSF-DMR-1056943).

- <sup>1</sup>A. D. Yoffe, *Adv. Phys.* **50**, 1 (2001).
- <sup>2</sup>P. Bhattacharya, S. Ghosh, and A. D. Stiff-Roberts, *Ann. Rev. Mater. Res.* **34**, 1 (2004).
- <sup>3</sup>R. Dingle, W. Wiegmann, and C. Henry, *Phys. Rev. Lett.* **33**, 827 (1974).
- <sup>4</sup>C. Murray, C. Kagan, and M. Bawendi, *Ann. Rev. Mater. Sci.* **30**, 545 (2000).
- <sup>5</sup>D. V. Talapin, J.-S. Lee, M. V. Kovalenko, and E. V. Shevchenko, *Chem. Rev.* **110**, 389 (2010).
- <sup>6</sup>Y. Yin and A. P. Alivisatos, *Nature* **437**, 664 (2005).
- <sup>7</sup>C. Collier, T. Vossmeyer, and J. Heath, *Ann. Rev. Phys. Chem.* **49**, 371 (1998).
- <sup>8</sup>A. Nozik, *Physica E* **14**, 115 (2002).
- <sup>9</sup>A. I. Boukai, Y. Bunimovich, J. Tahir-Kheli, J. K. Yu, W. A. Goddard, and J. R. Heath, *Nature* **451**, 168 (2008).
- <sup>10</sup>L. D. Hicks and M. S. Dresselhaus, *Phys. Rev. B* **47**, 12727 (1993).
- <sup>11</sup>L. D. Hicks and M. S. Dresselhaus, *Phys. Rev. B* **47**, 16631 (1993).
- <sup>12</sup>L. D. Hicks, T. C. Harman, and M. S. Dresselhaus, *Appl. Phys. Lett.* **63**, 3230 (1993).
- <sup>13</sup>A. I. Hochbaum, R. K. Chen, R. D. Delgado, W. J. Liang, E. C. Garnett, M. Najarian, A. Majumdar, and P. D. Yang, *Nature* **451**, 163 (2008).
- <sup>14</sup>K. F. Hsu, S. Loo, F. Guo, W. Chen, J. S. Dyck, C. Uher, T. Hogan, E. K. Polychroniadis, and M. G. Kanatzidis, *Science* **303**, 818 (2004).
- <sup>15</sup>R. Venkatasubramanian, E. Siivola, T. Colpitts, and B. O'Quinn, *Nature* **413**, 597 (2001).
- <sup>16</sup>R. Y. Wang, J. P. Feser, J. S. Lee, D. V. Talapin, R. Segalman, and A. Majumdar, *Nano Lett.* **8**, 2283 (2008).
- <sup>17</sup>G. D. Mahan and J. O. Sofo, *Proc. Natl. Acad. Sci. USA* **93**, 7436 (1996).
- <sup>18</sup>T. E. Humphrey and H. Linke, *Phys. Rev. Lett.* **94**, 7436 (2005).
- <sup>19</sup>T. M. Tritt, H. Boettner, and L. Chen, *MRS Bull.* **33**, 366 (2008).
- <sup>20</sup>W. Kim, R. Wang, and A. Majumdar, *Nano Today* **2**, 40 (2007).
- <sup>21</sup>G. J. Snyder and E. S. Toberer, *Nat. Mater.* **7**, 105 (2008).
- <sup>22</sup>J. Baxter *et al.*, *Energy Environ. Sci.* **2**, 559 (2009).
- <sup>23</sup>D. Milliron, I. Gur, and A. Alivisatos, *Mrs Bull.* **30**, 41 (2005).
- <sup>24</sup>A. J. Nozik, M. C. Beard, J. M. Luther, M. Law, R. J. Ellingson, and J. C. Johnson, *Chem. Rev.* **110**, 6873 (2010).
- <sup>25</sup>A. L. Rogach *et al.*, *Angew. Chem. Int. Ed.* **47**, 6538 (2008).
- <sup>26</sup>N. Gaponik, S. G. Hickey, D. Dorfs, A. L. Rogach, and A. Eychmuller, *Small* **6**, 1364 (2010).
- <sup>27</sup>C. J. Vineis, A. Shakouri, A. Majumdar, and M. G. Kanatzidis, *Adv. Mater.* **22**, 3970 (2010).
- <sup>28</sup>Z.-Y. Zhou, N. Tian, J.-T. Li, I. Broadwell, and S.-G. Sun, *Chem. Soc. Rev.* **40**, 4167 (2011).
- <sup>29</sup>A. Arico, P. Bruce, B. Scrosati, J. Tarascon, and W. van Schalkwijk, *Nat. Mater.* **4**, 366 (2005).
- <sup>30</sup>P. G. Bruce, B. Scrosati, and J.-M. Tarascon, *Angew. Chem. Int. Ed.* **47**, 2930 (2008).
- <sup>31</sup>A. T. Bell, *Science* **299**, 1688 (2003).
- <sup>32</sup>R. Narayanan and M. A. El-Sayed, *J. Phys. Chem. B* **109**, 12663 (2005).
- <sup>33</sup>M. Bruchez, M. Moronne, P. Gin, S. Weiss, and A. P. Alivisatos, *Science* **281**, 2013 (1998).
- <sup>34</sup>X. Michalet *et al.*, *Science* **307**, 538 (2005).
- <sup>35</sup>V. I. Klimov, *Nanocrystal Quantum Dots*, 2nd ed. (CRC, Boca Raton, 2009).
- <sup>36</sup>G. Markovich, C. P. Collier, S. E. Henrichs, F. o. Remacle, R. D. Levine, and J. R. Heath, *Acc. Chem. Res.* **32**, 415 (1999).
- <sup>37</sup>T. Vossmeyer, G. Reck, L. Katsikas, E. T. K. Haupt, B. Schulz, and H. A. Waller, *Science* **267**, 1476 (1995).
- <sup>38</sup>G. Bryant, *Phys. Rev. B* **40**, 1620 (1989).
- <sup>39</sup>C. Murray, C. Kagan, and M. Bawendi, *Science* **270**, 1335 (1995).
- <sup>40</sup>G. Springholz, V. Holy, M. Pinczelits, and G. Bauer, *Science* **282**, 734 (1998).
- <sup>41</sup>G. D. Stucky and J. E. Macdougall, *Science* **247**, 669 (1990).
- <sup>42</sup>D. A. McQuarrie and J. D. Simon, *Physical Chemistry: A Molecular Approach* (University Science Books, Sausalito, 1997).
- <sup>43</sup>K. Beverly, J. Sample, J. Sampaio, F. Remacle, J. Heath, and R. Levine, *Proc. Natl. Acad. Sci. USA* **99**, 6456 (2002).
- <sup>44</sup>A. Bartnik, A. Efros, W. K. Koh, C. Murray, and F. Wise, *Phys. Rev. B* **82**, 195313 (2010).
- <sup>45</sup>K.-S. Cho, D. V. Talapin, W. Gaschler, and C. B. Murray, *J. Am. Chem. Soc.* **127**, 7140 (2005).
- <sup>46</sup>S. Kan, T. Mokari, E. Rothenberg, and U. Banin, *Nat. Mater.* **2**, 155 (2003).
- <sup>47</sup>C. Schliehe *et al.*, *Science* **329**, 550 (2010).
- <sup>48</sup>W. Buhro and V. Colvin, *Nat. Mater.* **2**, 138 (2003).
- <sup>49</sup>L. Brus, *J. Chem. Phys.* **80**, 4403 (1984).
- <sup>50</sup>A. L. Efros and A. L. Efros, *Sov. Phys. Semicond.* **16**, 772 (1982).
- <sup>51</sup>A. Fojtik, H. Weller, U. Koch, and A. Henglein, *Bunsen-Ges. Phys. Chem. Chem. Phys.* **88**, 969 (1984).
- <sup>52</sup>L. Brus, *J. Chem. Phys.* **79**, 5566 (1983).
- <sup>53</sup>L.-W. Wang and A. Zunger, *Phys. Rev. B* **53**, 9579 (1996).
- <sup>54</sup>P. E. Lippens and M. Lannoo, *Phys. Rev. B* **41**, 6079 (1990).
- <sup>55</sup>S. Öğüt, J. Chelikowsky, and S. Louie, *Phys. Rev. Lett.* **79**, 1770 (1997).
- <sup>56</sup>F. W. Wise, *Acc. Chem. Res.* **33**, 773 (2000).
- <sup>57</sup>U. Gnatzmann and K. Clausecker, *Appl. Phys. A* **3**, 9 (1974).
- <sup>58</sup>C. Menoni, L. Miao, D. Patel, O. Mic'ic, and A. Nozik, *Phys. Rev. Lett.* **84**, 4168 (2000).
- <sup>59</sup>M. T. Trinh, A. J. Houtepen, J. M. Schins, J. Piris, and L. D. A. Siebbeles, *Nano Lett.* **8**, 2112 (2008).
- <sup>60</sup>P. Liljeroth, L. Jdira, K. Overgaag, B. Grandidier, S. Speller, and D. L. Vanmaekelbergh, *Phys. Chem. Chem. Phys.* **8**, 3845 (2006).
- <sup>61</sup>G. Schedelbeck, W. Wegscheider, and M. Bichler, *Science* **278**, 1792 (1997).
- <sup>62</sup>A. Zabet-Khosousi and A.-A. Dhirani, *Chem. Rev.* **108**, 4072 (2008).
- <sup>63</sup>N. F. Mott, *Conduction in Non-crystalline Materials*, 2nd ed. (Clarendon, Oxford, 1993).
- <sup>64</sup>C. Jiang and M. Green, *J. Appl. Phys.* **99**, 114902 (2006).
- <sup>65</sup>O. Lazarenkova and A. Balandin, *J. Appl. Phys.* **89**, 5509 (2001).
- <sup>66</sup>D. L. Nika, E. P. Pokatilov, Q. Shao, and A. A. Balandin, *Phys. Rev. B* **76**, 125417 (2007).
- <sup>67</sup>T. Takagahara, *Surf. Sci.* **267**, 310 (1992).
- <sup>68</sup>T. H. Oosterkamp, T. Fujisawa, W. G. van der Wiel, K. Ishibashi, R. V. Hijman, S. Tarucha, and L. P. Kouwenhoven, *Nature* **395**, 873 (1998).
- <sup>69</sup>A. Lagendijk, B. Van Tiggelen, and D. S. Wiersma, *Phys. Today* **62**, 24 (2009).
- <sup>70</sup>I. Gomez, F. Dominguez-Adame, E. Diez, and P. Orellana, *J. Appl. Phys.* **92**, 4486 (2002).
- <sup>71</sup>B. Smith and A. Nozik, *Nano Lett.* **1**, 36 (2001).
- <sup>72</sup>F. Remacle and R. Levine, *J. Phys. Chem. B* **105**, 2153 (2001).
- <sup>73</sup>M. A. El-Sayed, *Acc. Chem. Res.* **34**, 257 (2001).
- <sup>74</sup>J. A. Tang and E. H. Sargent, *Adv. Mater.* **23**, 12 (2011).
- <sup>75</sup>W. A. Tisdale, K. J. Williams, B. A. Timp, D. J. Norris, E. S. Aydil, and X. Y. Zhu, *Science* **328**, 1543 (2010).
- <sup>76</sup>R. D. Schaller and V. I. Klimov, *Phys. Rev. Lett.* **92**, 186601/1 (2004).
- <sup>77</sup>R. J. Ellingson, M. C. Beard, J. C. Johnson, P. Yu, O. I. Micic, A. J. Nozik, A. Shabaev, and A. L. Efros, *Nano Lett.* **5**, 865 (2005).
- <sup>78</sup>G. Nair and M. Bawendi, *Phys. Rev. B* **76**, 4 (2007).
- <sup>79</sup>M. Ben-Lulu, D. Mocatta, M. Bonn, U. Banin, and S. Ruhman, *Nano Lett.* **8**, 1207 (2008).

- <sup>80</sup>J. A. McGuire, J. Joo, J. Pietryga, R. Schaller, and V. I. Klimov, *Acc. Chem. Res.* **41**, 1810 (2008).
- <sup>81</sup>M. C. Beard, A. G. Midgett, M. Law, O. E. Semonin, R. J. Ellingson, and A. J. Nozik, *Nano Lett.* **9**, 836 (2009).
- <sup>82</sup>G. Allan and C. Delerue, *Phys. Rev. B* **79**, 5 (2009).
- <sup>83</sup>A. Shabaev, A. L. Efros, and A. J. Nozik, *Nano Lett.* **6**, 2856 (2006).
- <sup>84</sup>J. A. McGuire, M. Sykora, J. Joo, J. M. Pietryga, and V. I. Klimov, *Nano Lett.* **10**, 2049 (2010).
- <sup>85</sup>M. C. Beard, A. G. Midgett, M. C. Hanna, J. M. Luther, B. K. Hughes, and A. J. Nozik, *Nano Lett.* **10**, 3019 (2010).
- <sup>86</sup>J. B. Sambur, T. Novet, and B. A. Parkinson, *Science* **330**, 63 (2010).
- <sup>87</sup>O. E. Semonin, J. M. Luther, S. Choi, H.-Y. Chen, J. Gao, A. J. Nozik, and M. C. Beard, *Science* **334**, 1530 (2011).
- <sup>88</sup>R. A. Marcus, *Rev. Mod. Phys.* **65**, 599 (1993).
- <sup>89</sup>I. Robel, M. Kuno, and P. V. Kamat, *J. Am. Chem. Soc.* **129**, 4136 (2007).
- <sup>90</sup>X. M. Jiang, R. D. Schaller, S. B. Lee, J. M. Pietryga, V. I. Klimov, and A. A. Zakhidov, *J. Mater. Res.* **22**, 2204 (2007).
- <sup>91</sup>H. Du, C. L. Chen, R. Krishnan, T. D. Krauss, J. M. Harbold, F. W. Wise, M. G. Thomas, and J. Silcox, *Nano Lett.* **2**, 1321 (2002).
- <sup>92</sup>J. M. Pietryga, R. D. Schaller, D. Werder, M. H. Stewart, V. I. Klimov, and J. A. Hollingsworth, *J. Am. Chem. Soc.* **126**, 11752 (2004).
- <sup>93</sup>D. Cui, J. Xu, T. Zhu, G. Paradee, and S. Ashok, *Appl. Phys. Lett.* **88**, 183111 (2006).
- <sup>94</sup>C. Evans, L. Guo, J. Peterson, S. Maccagnano-Zacher, and T. Krauss, *Nano Lett.* **8**, 2896 (2008).
- <sup>95</sup>Z. Zhu, E. Kurtz, K. Arai, Y. Chen, D. Bagnall, P. Tomashini, F. Lu, T. Sekiguchi, T. Yao, and T. Yasuda, *Physica Status Solidi B* **202**, 827 (1997).
- <sup>96</sup>H. Omi and T. Ogino, *Phys. Rev. B* **59**, 7521 (1999).
- <sup>97</sup>D. J. Eglesham and M. Cerullo, *Phys. Rev. Lett.* **64**, 1943 (1990).
- <sup>98</sup>C. Teichert, *Phys Rep.* **365**, 335 (2002).
- <sup>99</sup>S. Guha, A. Madhukar, and K. C. Rajkumar, *Appl. Phys. Lett.* **57**, 2110 (1990).
- <sup>100</sup>C. W. Snyder, B. G. Orr, D. Kessler, and L. M. Sander, *Phys. Rev. Lett.* **66**, 3032 (1991).
- <sup>101</sup>M. K. Zundel, P. Specht, K. Eberl, N. Y. JinPhillipp, and F. Phillip, *Appl. Phys. Lett.* **71**, 2972 (1997).
- <sup>102</sup>M. C. Hanna, Z. H. Lu, A. F. Cahill, M. J. Heben, and A. J. Nozik, *J. Cryst. Growth* **174**, 605 (1997).
- <sup>103</sup>C. B. Murray, D. J. Norris, and M. G. Bawendi, *J. Am. Chem. Soc.* **115**, 8706 (1993).
- <sup>104</sup>S. G. Kwon and T. Hyeon, *Small* **7**, 2685 (2011).
- <sup>105</sup>A. Henglein, *Ber. Bunsen-Ges. Phys. Chem. Chem. Phys.* **86**, 301 (1982).
- <sup>106</sup>L. Mangolini, E. Thimsen, and U. Kortshagen, *Nano Lett.* **5**, 655 (2005).
- <sup>107</sup>P. Shah, T. Hanrath, K. Johnston, and B. Korgel, *J. Phys. Chem. B* **108**, 9574 (2004).
- <sup>108</sup>N. F. Borrelli and D. W. Smith, *J. Non-Cryst. Solids* **180**, 25 (1994).
- <sup>109</sup>A. L. Rogach, *Semiconductor Nanocrystal Quantum Dots: Synthesis, Assembly, Spectroscopy and Applications* (Springer, Wien, 2008).
- <sup>110</sup>V. K. Lamer and R. H. Dinegar, *J. Am. Chem. Soc.* **72**, 4847 (1950).
- <sup>111</sup>T. Sugimoto, *Adv. Colloid. Interface* **28**, 65 (1987).
- <sup>112</sup>I. Moreels, B. Fritzinger, J. C. Martins, and Z. Hens, *J. Am. Chem. Soc.* **130**, 15081 (2008).
- <sup>113</sup>I. C. Baek, S. I. Seok, N. C. Pramanik, S. Jana, M. A. Lim, B. Y. Ahn, C. J. Lee, and Y. J. Jeong, *J. Colloid Interf. Sci.* **310**, 163 (2007).
- <sup>114</sup>S. Abe, R. K. Čapek, B. De Geyter, and Z. Hens, *ACS Nano* **6**, 42 (2011).
- <sup>115</sup>T. P. Martin, *Phys. Rep.* **273**, 199 (1996).
- <sup>116</sup>C. M. Evans, L. Guo, J. J. Peterson, S. Maccagnano-Zacher, and T. D. Krauss, *Nano Lett.* **8**, 2896 (2008).
- <sup>117</sup>H. Zheng, R. K. Smith, Y.-w. Jun, C. Kisielowski, U. Dahmen, and A. P. Alivisatos, *Science* **324**, 1309 (2009).
- <sup>118</sup>S. Polarz, *Adv. Funct. Mater.* **21**, 3214 (2011).
- <sup>119</sup>L. Manna, E. Scher, and A. Alivisatos, *J. Am. Chem. Soc.* **122**, 12700 (2000).
- <sup>120</sup>F. Wang, R. Tang, and W. E. Buhro, *Nano Lett.* **8**, 3521 (2008).
- <sup>121</sup>A. Houtepen, R. Koole, D. Vanmaekelbergh, and J. Meeldijk, *J. Am. Chem. Soc.* **128**, 6792 (2006).
- <sup>122</sup>Q. Pang *et al.*, *Chem Mater* **17**, 5263 (2005).
- <sup>123</sup>L. Manna, D. J. Milliron, A. Meisel, E. C. Scher, and A. P. Alivisatos, *Nat. Mater.* **2**, 382 (2003).
- <sup>124</sup>J. Q. Hu, Y. Bando, and D. Golberg, *Small* **1**, 95 (2005).
- <sup>125</sup>Y. C. Zhu, Y. Bando, D. F. Xue, and D. Golberg, *J. Am. Chem. Soc.* **125**, 16196 (2003).
- <sup>126</sup>B. Fritzinger, R. K. Čapek, K. Lambert, J. C. Martins, and Z. Hens, *J. Am. Chem. Soc.* **132**, 10195 (2010).
- <sup>127</sup>B. Fritzinger, I. Moreels, P. Lommens, R. Koole, Z. Hens, and J. C. Martins, *J. Am. Chem. Soc.* **131**, 3024 (2009).
- <sup>128</sup>M. B. Mohamed, C. Burda, and M. A. El-Sayed, *Nano Lett.* **1**, 589 (2001).
- <sup>129</sup>J. Hu, L.-s. Li, W. Yang, L. Manna, L.-w. Wang, and A. P. Alivisatos, *Science* **292**, 2060 (2001).
- <sup>130</sup>B.-R. Hyun, A. C. Bartnik, W.-k. Koh, N. I. Agladze, J. P. Wrubel, A. J. Sievers, C. B. Murray, and F. W. Wise, *Nano Lett.* **11**, 2786 (2011).
- <sup>131</sup>X. Peng, M. C. Schlamp, A. V. Kadavanich, and A. P. Alivisatos, *J. Am. Chem. Soc.* **119**, 7019 (1997).
- <sup>132</sup>A. Pandey and P. Guyot-Sionnest, *Science* **322**, 929 (2008).
- <sup>133</sup>L. Carbone *et al.*, *Nano Lett.* **7**, 2942 (2007).
- <sup>134</sup>P. D. Cozzoli, T. Pellegrino, and L. Manna, *Chem. Soc. Rev.* **35**, 1195 (2006).
- <sup>135</sup>S. Kumar, M. Jones, S. S. Lo, and G. D. Scholes, *Small* **3**, 1633 (2007).
- <sup>136</sup>K. Becker, J. M. Lupton, J. Muller, A. L. Rogach, D. V. Talapin, H. Weller, and J. Feldmann, *Nat. Mater.* **5**, 777 (2006).
- <sup>137</sup>M. Sykora, A. Y. Koposov, J. A. McGuire, R. K. Schulze, O. Tretiak, J. M. Pietryga, and V. I. Klimov, *ACS Nano* **4**, 2021 (2010).
- <sup>138</sup>S. N. Inamdar, P. P. Ingole, and S. K. Haram, *Chemphyschem* **9**, 2574 (2008).
- <sup>139</sup>J. J. Choi *et al.*, *Nano Lett.* **9**, 3749 (2009).
- <sup>140</sup>V. Colvin, A. Alivisatos, and J. Tobin, *Phys. Rev. Lett.* **66**, 2786 (1991).
- <sup>141</sup>J. Jasieniak, M. Califano, and S. Watkins, *ACS Nano* **5**, 5888 (2011).
- <sup>142</sup>A. M. Munro, B. Zacher, A. Graham, and N. R. Armstrong, *ACS Appl. Mater. Int.* **2**, 863 (2010).
- <sup>143</sup>B. A. Timp and X. Y. Zhu, *Surf. Sci.* **604**, 1335 (2010).
- <sup>144</sup>R. Cohen, L. Kronik, A. Shanzer, D. Cahen, A. Liu, Y. Rosenwaks, J. K. Lorenz, and A. B. Ellis, *J. Am. Chem. Soc.* **121**, 10545 (1999).
- <sup>145</sup>M. Soreni-Harari, N. Yaacobi-Gross, D. Steiner, A. Aharoni, U. Banin, O. Millo, and N. Tessler, *Nano Lett.* **8**, 678 (2008).
- <sup>146</sup>A. Kongkanand, K. Tvrdy, K. Takechi, M. Kuno, and P. V. Kamat, *J. Am. Chem. Soc.* **130**, 4007 (2008).
- <sup>147</sup>F. Xu, X. Ma, C. R. Haughn, J. Benavides, M. F. Doty, and S. G. Cloutier, *ACS Nano* **5**, 9950 (2011).
- <sup>148</sup>I. J. Kramer, L. Levina, R. Debnath, D. Zhitomirsky, and E. H. Sargent, *Nano Lett.* **11**, 3701 (2011).
- <sup>149</sup>J. J. Choi, W. N. Wenger, R. S. Hoffman, Y.-F. Lim, J. Luria, J. Jasieniak, J. A. Marohn, and T. Hanrath, *Adv. Mater.* **23**, 3144 (2011).
- <sup>150</sup>X. Wang *et al.*, *Nat. Photon.* **5**, 480 (2011).
- <sup>151</sup>F. Remacle and R. Levine, *Chemphyschem* **2**, 20 (2001).
- <sup>152</sup>E. V. Shevchenko, D. V. Talapin, N. A. Kotov, S. O'Brien, and C. B. Murray, *Nature* **439**, 55 (2006).
- <sup>153</sup>B. Lee, P. Podsiadlo, S. Rupich, D. V. Talapin, T. Rajh, and E. V. Shevchenko, *J. Am. Chem. Soc.* **131**, 16386 (2009).
- <sup>154</sup>N. J. Tao, *Nat. Nano* **1**, 173 (2006).
- <sup>155</sup>D. Yu, C. Wang, and P. Guyot-Sionnest, *Science* **300**, 1277 (2003).
- <sup>156</sup>D. V. Talapin and C. B. Murray, *Science* **310**, 86 (2005).
- <sup>157</sup>M. Law, J. M. Luther, Q. Song, B. K. Hughes, C. L. Perkins, and A. J. Nozik, *J. Am. Chem. Soc.* **130**, 5974 (2008).
- <sup>158</sup>J. J. Choi, J. Luria, B.-R. Hyun, A. C. Bartnik, L. Sun, Y.-F. Lim, J. A. Marohn, F. W. Wise, and T. Hanrath, *Nano Lett.* **10**, 1805 (2010).
- <sup>159</sup>A. Wolcott *et al.*, *J. Phys. Chem. Lett.* **2**, 795 (2011).
- <sup>160</sup>Y. Liu, M. Gibbs, J. Puthussery, S. Gaik, R. Ihly, H. W. Hillhouse, and M. Law, *Nano Lett.* **10**, 1960 (2010).
- <sup>161</sup>M. H. Zarghami, Y. Liu, M. Gibbs, E. Gebremichael, C. Webster, and M. Law, *ACS Nano* **4**, 2475 (2010).
- <sup>162</sup>J. M. Luther, M. Law, Q. Song, C. L. Perkins, M. C. Beard, and A. J. Nozik, *ACS Nano* **2**, 271 (2008).
- <sup>163</sup>S. Kitada, E. Kikuchi, A. Ohno, S. Aramaki, and S. Maenosono, *Solid State Commun.* **149**, 1853 (2009).
- <sup>164</sup>Y. Gao, E. Talgorn, M. Aerts, M. T. Trinh, J. M. Schins, A. J. Houtepen, and L. D. A. Siebbeles, *Nano Lett.* **11**, 5471 (2011).
- <sup>165</sup>G. Sarasqueta, K. R. Choudhury, and F. So, *Chem. Mater.* **22**, 3496 (2010).
- <sup>166</sup>G. I. Koleilat, L. Levina, H. Shukla, S. H. Myrskog, S. Hinds, A. G. Patantayus-Abraham, and E. H. Sargent, *ACS Nano* **2**, 833 (2008).
- <sup>167</sup>K. S. Jeong *et al.*, *ACS Nano* **6**, 89 (2011).
- <sup>168</sup>V. Wood, M. J. Panzer, D. Bozyigit, Y. Shirasaki, I. Rousseau, S. Geyer, M. G. Bawendi, and V. Bulović, *Nano Lett.* **11**, 2927 (2011).

- <sup>169</sup>B.-R. Hyun, A. C. Bartnik, L. Sun, T. Hanrath, and F. W. Wise, *Nano Lett.* **11**, 2126 (2011).
- <sup>170</sup>L. Etgar, J. H. Park, C. Barolo, M. K. Nazeeruddin, G. Viscardi, and M. Graetzel, *ACS Appl. Mater. Int.* **3**, 3264 (2011).
- <sup>171</sup>M. V. Kovalenko, M. Scheele, and D. V. Talapin, *Science* **324**, 1417 (2009).
- <sup>172</sup>D. B. Mitzi, L. L. Kosbar, C. E. Murray, M. Copel, and A. Afzali, *Nature* **428**, 299 (2004).
- <sup>173</sup>R. Tangirala, J. L. Baker, A. P. Alivisatos, and D. J. Milliron, *Angew. Chem. Int. Ed.* **49**, 2878 (2010).
- <sup>174</sup>A. Nag, M. V. Kovalenko, J.-S. Lee, W. Liu, B. Spokoyny, and D. V. Talapin, *J. Am. Chem. Soc.* **133**, 10612 (2011).
- <sup>175</sup>H. Zhang, B. Hu, L. Sun, R. Hovden, F. W. Wise, D. A. Muller, and R. D. Robinson, *Nano Lett.* **11**, 5356 (2011).
- <sup>176</sup>J. Tang *et al.*, *Nat. Mater.* **10**, 765 (2011).
- <sup>177</sup>A. Pourret, P. Guyot-Sionnest, and J. W. Elam, *Adv. Mater.* **21**, 232 (2008).
- <sup>178</sup>E. M. Likovich, R. Jaramillo, K. J. Russell, S. Ramanathan, and V. Narayanamurti, *Adv. Mater.* **23**, 4521 (2011).
- <sup>179</sup>R. Ihly, J. Tolentino, Y. Liu, M. Gibbs, and M. Law, *ACS Nano* **5**, 8175 (2011).
- <sup>180</sup>Y. Liu, M. Gibbs, C. L. Perkins, J. Tolentino, M. H. Zarghami, J. Bustamante, and M. Law, *Nano Lett.* **11**, 5349 (2011).
- <sup>181</sup>I. Gur, N. Fromer, M. Geier, and A. Alivisatos, *Science* **310**, 462 (2005).
- <sup>182</sup>Z. Wang, C. Schliehe, T. Wang, Y. Nagaoka, Y. C. Cao, W. A. Bassett, H. Wu, H. Fan, and H. Weller, *J. Am. Chem. Soc.* **133**, 14484 (2011).
- <sup>183</sup>H. Wu, F. Bai, Z. Sun, R. E. Haddad, D. M. Boye, Z. Wang, J. Y. Huang, and H. Fan, *J. Am. Chem. Soc.* **132**, 12826 (2010).
- <sup>184</sup>L. Cademartiri, A. Ghadimi, and G. A. Ozin, *Acc. Chem. Res.* **41**, 1820 (2008).
- <sup>185</sup>M. Drndic, M. V. Jarosz, N. Y. Morgan, M. A. Kastner, and M. G. Bawendi, *J. Appl. Phys.* **92**, 7498 (2002).
- <sup>186</sup>B. W. Goodfellow, R. N. Patel, M. G. Panthani, D.-M. Smilgies, and B. A. Korgel, *J. Phys. Chem. C* **115**, 6397 (2011).
- <sup>187</sup>P. Liljeroth, K. Overgaag, A. Urbietta, B. Grandidier, S. G. Hickey, and D. I. Vanmaekelbergh, *Phys. Rev. Lett.* **97**, 096803 (2006).
- <sup>188</sup>T. S. Mentzel, V. J. Porter, S. Geyer, K. MacLean, M. G. Bawendi, and M. A. Kastner, *Phys. Rev. B* **77**, 075316 (2008).
- <sup>189</sup>S. J. Baik, K. Kim, K. S. Lim, S. Jung, Y.-C. Park, D. G. Han, S. Lim, S. Yoo, and S. Jeong, *J. Phys. Chem. C* **115**, 607 (2011).
- <sup>190</sup>A. Dong, J. Chen, P. M. Vora, J. M. Kikkawa, and C. B. Murray, *Nature* **466**, 474 (2010).
- <sup>191</sup>E. J. D. Klem, H. Shukla, S. Hinds, D. D. MacNeil, L. Levina, and E. H. Sargent, *Appl. Phys. Lett.* **92**, 212105 (2008).
- <sup>192</sup>V. J. Porter, S. Geyer, J. E. Halpert, M. A. Kastner, and M. G. Bawendi, *J. Phys. Chem. C* **112**, 2308 (2008).
- <sup>193</sup>H. E. Romero and M. Drndic, *Phys. Rev. Lett.* **95**, 156801 (2005).
- <sup>194</sup>M. A. van Huis, L. T. Kunneman, K. Overgaag, Q. Xu, G. Pandraud, H. W. Zandbergen, and D. Vanmaekelbergh, *Nano Lett.* **8**, 3959 (2008).
- <sup>195</sup>W. J. Baumgardner, J. J. Choi, K. Bian, L. Fitting Kourkoutis, D.-M. Smilgies, M. O. Thompson, and T. Hanrath, *ACS Nano* **5**, 7010 (2011).
- <sup>196</sup>C. P. Collier, R. J. Saykally, J. J. Shiang, S. E. Henrichs, and J. R. Heath, *Science* **277**, 1978 (1997).
- <sup>197</sup>A. Tao, P. Sinsermsuksakul, and P. Yang, *Nat. Nano* **2**, 435 (2007).
- <sup>198</sup>A. R. Tao, J. Huang, and P. Yang, *Acc. Chem. Res.* **41**, 1662 (2008).
- <sup>199</sup>P. Podsiadlo, B. Lee, V. B. Prakapenka, G. V. Krylova, R. D. Schaller, A. Demortiere, and E. V. Shevchenko, *Nano Lett.* **11**, 579 (2011).
- <sup>200</sup>D. C. Sayle *et al.*, *ACS Nano* **2**, 1237 (2008).
- <sup>201</sup>S. Hegedus, *Prog. Photovoltaics* **14**, 393 (2006).
- <sup>202</sup>X. M. Lin, H. M. Jaeger, C. M. Sorensen, and K. J. Klabunde, *J. Phys. Chem. B* **105**, 3353 (2001).
- <sup>203</sup>R. J. Macfarlane, B. Lee, M. R. Jones, N. Harris, G. C. Schatz, and C. A. Mirkin, *Science* **334**, 204 (2011).
- <sup>204</sup>E. V. Shevchenko, D. V. Talapin, N. A. Kotov, S. O'Brien, and C. B. Murray, *Nature* **439**, 55 (2006).
- <sup>205</sup>W. H. Evers, H. Friedrich, L. Filion, M. Dijkstra, and D. Vanmaekelbergh, *Angew. Chem. Int. Ed.* **48**, 9655 (2009).
- <sup>206</sup>Z. Quan and J. Fang, *Nano Today* **5**, 390 (2010).
- <sup>207</sup>K. Miszta *et al.*, *Nat. Mater.* **10**, 872 (2011).
- <sup>208</sup>Y. Xia, T. D. Nguyen, M. Yang, B. Lee, A. Santos, P. Podsiadlo, Z. Tang, S. C. Glotzer, and N. A. Kotov, *Nat. Nanotechnol.* **6**, 580 (2011).
- <sup>209</sup>M. P. Pileni, *J. Phys. Chem. B* **105**, 3358 (2001).
- <sup>210</sup>N. A. Kotov, *Nanoparticle Assemblies and Superstructures* (CRC Press, Boca Raton, 2006).
- <sup>211</sup>K. J. M. Bishop, C. E. Wilmer, S. Soh, and B. A. Grzybowski, *Small* **5**, 1600 (2009).
- <sup>212</sup>W. H. Evers, B. de Nijs, L. Filion, S. Castillo, M. Dijkstra, and D. Vanmaekelbergh, *Nano Lett.* **10**, 4235 (2010).
- <sup>213</sup>B. Korgel and D. Fitzmaurice, *Phys. Rev. B* **59**, 14191 (1999).
- <sup>214</sup>R. L. Whetten, M. N. Shafiqullin, J. T. Khouri, T. G. Schaaff, I. Vezmar, M. M. Alvarez, and A. Wilkinson, *Acc. Chem. Res.* **32**, 397 (1999).
- <sup>215</sup>S. C. Glotzer, M. J. Solomon, and N. A. Kotov, *AIChE J.* **50**, 2978 (2004).
- <sup>216</sup>J. Henzie, M. Grünwald, A. Widmer-Cooper, P. L. Geissler, and P. Yang, *Nat. Mater.* **11**, 131 (2011).
- <sup>217</sup>P. F. Damasceno, M. Engel, and S. C. Glotzer, *ACS Nano* **6**, 609 (2011).
- <sup>218</sup>K. Bian, J. J. Choi, A. Kaushik, P. Clancy, D.-M. Smilgies, and T. Hanrath, *ACS Nano* **5**, 2815 (2011).
- <sup>219</sup>E. Bain, *Trans. Am. Inst. Miner. Met. Eng.* **70**, 25 (1924).
- <sup>220</sup>J. J. Choi, C. R. Bealing, K. Bian, K. J. Hughes, W. Zhang, D.-M. Smilgies, R. G. Hennig, J. R. Engstrom, and T. Hanrath, *J. Am. Chem. Soc.* **133**, 3131 (2011).
- <sup>221</sup>Y. Zhang, F. Lu, D. van der Lelie, and O. Gang, *Phys. Rev. Lett.* **107**, (2011).
- <sup>222</sup>M. C. Troparevsky, K. Zhao, D. Xiao, A. G. Eguiluz, and Z. Zhang, *Phys. Rev. B* **82**, 045413 (2010).
- <sup>223</sup>S. Auer and D. Frenkel, *Nature* **413**, 711 (2001).
- <sup>224</sup>M. Shim and P. Guyot-Sionnest, *J. Chem. Phys.* **111**, 6955 (1999).
- <sup>225</sup>M. Klokkenburg, A. J. Houtepen, R. Koole, J. W. J. de Folter, B. H. Erne, E. van Faassen, and D. Vanmaekelbergh, *Nano Lett.* **7**, 2931 (2007).
- <sup>226</sup>T. Hanrath, D. Veldman, J. J. Choi, C. G. Christova, M. M. Wienk, and R. A. J. Janssen, *ACS Appl. Mater. Int.* **1**, 244 (2009).
- <sup>227</sup>D. V. Talapin, E. V. Shevchenko, C. B. Murray, A. V. Titov, and P. Kral, *Nano Lett.* **7**, 1213 (2007).
- <sup>228</sup>I. Moreels, B. Fritzinger, J. Martins, and Z. Hens, *J. Am. Chem. Soc.* **130**, 15081 (2008).
- <sup>229</sup>C. Fang, M. A. van Huis, D. Vanmaekelbergh, and H. W. Zandbergen, *ACS Nano* **4**, 211 (2010).
- <sup>230</sup>P. Bartlett, R. H. Ottewill, and P. N. Pusey, *Phys. Rev. Lett.* **68**, 3801 (1992).
- <sup>231</sup>D. Dunphy, H. Fan, X. Li, J. Wang, and C. J. Brinker, *Langmuir* **24**, 10575 (2008).
- <sup>232</sup>A. Abécassis, F. Testard, and O. Spalla, *Phys. Rev. Lett.* **100**, 115504 (2008).
- <sup>233</sup>Z. Jiang, X.-M. Lin, M. Sprung, S. Narayanan, and J. Wang, *Nano Lett.* **10**, 799 (2010).
- <sup>234</sup>T. Hanrath, J. J. Choi, and D. Smilgies, *ACS Nano* **3**, 2975 (2009).
- <sup>235</sup>S. Narayanan, J. Wang, and X. Lin, *Phys. Rev. Lett.* **93**, 135503 (2004).
- <sup>236</sup>V. L. Colvin, A. N. Goldstein, and A. P. Alivisatos, *J. Am. Chem. Soc.* **114**, 5221 (1992).
- <sup>237</sup>Z. Y. Tang, Z. L. Zhang, Y. Wang, S. C. Glotzer, and N. A. Kotov, *Science* **314**, 274 (2006).
- <sup>238</sup>S. Coe-Sullivan, J. S. Steckel, W. K. Woo, M. G. Bawendi, and V. Bulovic, *Adv. Funct. Mater.* **15**, 1117 (2005).
- <sup>239</sup>M. B. Sigman, A. E. Saunders, and B. A. Korgel, *Langmuir* **20**, 978 (2004).
- <sup>240</sup>L. Li and R. F. Ismagilov, *Annu. Rev. Biophys.* **39**, 139 (2010).
- <sup>241</sup>D. Talapin, E. Shevchenko, A. Kornowski, N. Gaponik, M. Haase, A. Rogach, and H. Weller, *Adv. Mater.* **13**, 1868 (2001).
- <sup>242</sup>M. I. Bodnarchuk, L. Li, A. Fok, S. Nachtergael, R. F. Ismagilov, and D. V. Talapin, *J. Am. Chem. Soc.* **133**, 8956 (2011).
- <sup>243</sup>S. Maenosono, T. Okubo, and Y. Yamaguchi, *J. Nanoparticle Res.* **5**, 5 (2003).
- <sup>244</sup>C. B. Murray, S. H. Sun, W. Gaschler, H. Doyle, T. A. Betley, and C. R. Kagan, *IBM J. Res. Dev.* **45**, 47 (2001).
- <sup>245</sup>Z. L. Wang, *Adv. Mater.* **10**, 13 (1998).
- <sup>246</sup>D. Smith, B. Goodfellow, D. Smilgies, and B. Korgel, *J. Am. Chem. Soc.* **131**, 3281 (2009).
- <sup>247</sup>T. Vossmeye, E. DeIonno, and J. R. Heath, *Angew. Chem. Int. Ed.* **36**, 1080 (1997).
- <sup>248</sup>A. G. Pattantyus-Abraham, H. Qiao, J. Shan, K. A. Abel, T.-S. Wang, F. C. J. M. van Veggel, and J. F. Young, *Nano Lett.* **9**, 2849 (2009).
- <sup>249</sup>H. Noh, C. Choi, A. M. Hung, S. Jin, and J. N. Cha, *ACS Nano* **4**, 5076 (2010).

- <sup>250</sup>Y. Cui, M. T. Björk, J. A. Liddle, C. Sönnichsen, B. Boussert, and A. P. Alivisatos, *Nano Lett.* **4**, 1093 (2004).
- <sup>251</sup>D. A. R. Barkhouse, R. Debnath, I. J. Kramer, D. Zhitomirsky, A. G. Pantanayus-Abraham, L. Levina, L. Etgar, M. Grätzel, and E. H. Sargent, *Adv. Mater.* **23**, 3134 (2011).
- <sup>252</sup>K. S. Leschkies, A. G. Jacobs, D. J. Norris, and E. S. Aydil, *Appl. Phys. Lett.* **95**, 193103 (2009).
- <sup>253</sup>P. Ball, *The Self-Made Tapestry: Pattern Formation in Nature* (Oxford University Press, Oxford, 1998).
- <sup>254</sup>E. H. Sargent, *IEEE J. Sel. Top. Quantum Electron.* **14**, 1223 (2008).
- <sup>255</sup>J. M. Luther, M. Law, M. C. Beard, Q. Song, M. O. Reese, R. J. Ellingson, and A. J. Nozik, *Nano Lett.* **8**, 3488 (2008).
- <sup>256</sup>C. J. Brinker, Y. F. Lu, A. Sellinger, and H. Y. Fan, *Adv. Mater.* **11**, 579 (1999).
- <sup>257</sup>E. Talgorn, M. A. de Vries, L. D. A. Siebbeles, and A. J. Houtepen, *ACS Nano* **5**, 3552 (2011).
- <sup>258</sup>B. Prevo and O. Velev, *Langmuir* **20**, 2099 (2004).
- <sup>259</sup>M. I. Bodnarchuk, M. V. Kovalenko, S. Pichler, G. Fritz-Popovski, G. Hesser, and W. Heiss, *ACS Nano* **4**, 423 (2010).
- <sup>260</sup>E. Tekin, P. J. Smith, S. Hoeppener, A. M. J. van den Berg, A. S. Susha, A. L. Rogach, J. Feldmann, and U. S. Schubert, *Adv. Funct. Mater.* **17**, 23 (2007).
- <sup>261</sup>M. Böberl, M. V. Kovalenko, S. Gamerith, E. J. W. List, and W. Heiss, *Adv. Mater.* **19**, 3574 (2007).
- <sup>262</sup>V. A. Akhavan, B. W. Goodfellow, M. G. Panthani, D. K. Reid, D. J. Hellebusch, T. Adachi, and B. A. Korgel, *Energy Environ. Sci.* **3**, 1600 (2010).
- <sup>263</sup>I. W. Lenggoro, H. M. Lee, and K. Okuyama, *J. Colloid Interf. Sci.* **303**, 124 (2006).
- <sup>264</sup>B. Dabbousi, C. Murray, M. Rubner, and M. Bawendi, *Chem. Mater.* **6**, 216 (1994).
- <sup>265</sup>K. Lambert, R. K. Capek, M. I. Bodnarchuk, M. V. Kovalenko, D. Van Thourhout, W. Heiss, and Z. Hens, *Langmuir* **26**, 7732 (2010).
- <sup>266</sup>A. Dong, X. Ye, J. Chen, and C. B. Murray, *Nano Lett.* **11**, 1804 (2011).
- <sup>267</sup>S. Pichler, M. I. Bodnarchuk, M. V. Kovalenko, M. Yarema, G. Springholz, D. V. Talapin, and W. Heiss, *ACS Nano* **5**, 1703 (2011).
- <sup>268</sup>S. Harfenist, Z. Wang, M. Alvarez, I. Vezmar, and R. Whetten, *J. Phys. Chem.* **100**, 13904 (1996).
- <sup>269</sup>H. Friedrich *et al.*, *Nano Lett.* **9**, 2719 (2009).
- <sup>270</sup>P. Guyot-Sionnest, in AIChE 2011 Annual Meeting, Minneapolis, Minnesota, 2011 (unpublished).
- <sup>271</sup>I. S. Beloborodov, A. V. Lopatin, V. M. Vinokur, and K. B. Efetov, *Rev. Mod. Phys.* **79**, 469 (2007).
- <sup>272</sup>D.-K. Ko, J. J. Urban, and C. B. Murray, *Nano Lett.* **10**, 1842 (2010).
- <sup>273</sup>A. L. Efros and B. I. Shklovskii, *J. Phys. C* **8**, L49 (1975).
- <sup>274</sup>B. Wehrenberg, D. Yu, J. Ma, and P. Guyot-Sionnest, *J. Phys. Chem. B* **109**, 20192 (2005).
- <sup>275</sup>A. J. Houtepen, D. Kockmann, and D. Vanmaekelbergh, *Nano Lett.* **8**, 3516 (2008).
- <sup>276</sup>D. Ginger and N. Greenham, *J. Appl. Phys.* **87**, 1361 (2000).
- <sup>277</sup>P. Nagpal and V. I. Klimov, *Nat. Commun.* **2**, 486 (2011).
- <sup>278</sup>G. Konstantatos, I. Howard, A. Fischer, S. Hoogland, J. Clifford, E. Klem, L. Levina, and E. Sargent, *Nature* **442**, 180 (2006).
- <sup>279</sup>D. A. R. Barkhouse, A. G. Pantantyus-Abraham, L. Levina, and E. H. Sargent, *ACS Nano* **2**, 2356 (2008).
- <sup>280</sup>I. Kramer and E. H. Sargent, *ACS Nano* **5**, 8506 (2011).
- <sup>281</sup>J. Lee, M. Kovalenko, J. Huang, D. Chung, and T. Dmitri, *Nature* **6**, 348 (2011).
- <sup>282</sup>E. Talgorn *et al.*, *Nat. Nanotech.* **6**, 733 (2011).
- <sup>283</sup>J. J. Urban, D. V. Talapin, E. V. Shevchenko, C. R. Kagan, and C. B. Murray, *Nat. Mater.* **6**, 115 (2007).
- <sup>284</sup>J. R. Heath, *Nature* **445**, 492 (2007).
- <sup>285</sup>J. Chen, A. Dong, J. Cai, X. Ye, Y. Kang, and C. Murray, *Nano Lett.* **10**, 5103 (2010).
- <sup>286</sup>H. Döllefeld, H. Weller, and A. Eychmuller, *J. Phys. Chem. B* **106**, 5604 (2002).
- <sup>287</sup>K. Overgaag, P. Liljeroth, B. Grandidier, and D. Vanmaekelbergh, *ACS Nano* **2**, 600 (2008).
- <sup>288</sup>D. V. Talapin and Y. Yin, *J. Mater. Chem.* **21**, 11454 (2011).
- <sup>289</sup>A. Chemseddine and H. Weller, *Ber. Bunsenges. Phys. Chem.* **97**, 636 (1993).
- <sup>290</sup>A. M. Al-Somali, K. M. Krueger, J. C. Falkner, and V. L. Colvin, *Anal. Chem.* **76**, 5903 (2004).
- <sup>291</sup>R. P. Carney, J. Y. Kim, H. Qian, R. Jin, H. Mehenni, F. Stellacci, and O. M. Bakr, *Nat. Commun.* **2**, 335 (2011).
- <sup>292</sup>S. Coe, W.-K. Woo, M. Bawendi, and V. Bulovic, *Nature* **420**, 800 (2002).
- <sup>293</sup>D. Zhitomirsky, I. J. Kramer, A. J. Labelle, A. Fischer, R. Debnath, J. Pan, O. M. Bakr, and E. H. Sargent, *Nano Lett.* **12**, 1007 (2012).
- <sup>294</sup>F. Hetsch, X. Xu, H. Wang, S. V. Kershaw, and A. L. Rogach, *J. Phys. Chem. Lett.* **2**, 1879 (2011).
- <sup>295</sup>S. C. Erwin, L. Zu, M. I. Haftel, A. L. Efros, T. A. Kennedy, and D. J. Norris, *Nature* **436**, 91 (2005).
- <sup>296</sup>G. M. Dalpian and J. R. Chelikowsky, *Phys. Rev. Lett.* **96**, 226802 (2006).
- <sup>297</sup>C. A. Wolden, J. Kurtin, J. B. Baxter, I. Repins, S. E. Shaheen, J. T. Torvik, A. A. Rockett, V. M. Fthenakis, and E. S. Aydil, *J. Vac. Sci. Technol. A* **29**, 030801 (2011).
- <sup>298</sup>C. Wadia, A. P. Alivisatos, and D. M. Kammen, *Environ. Sci. Technol.* **43**, 2072 (2009).